Supercritical Water Treatment of Crude Oil and Hexylbenzene: An Experimental and Mechanistic Study on Alkylbenzene Decomposition

Citation: Carr, Adam G. et al. "Supercritical Water Treatment of Crude Oil and Hexylbenzene: An Experimental and Mechanistic Study on Alkylbenzene Decomposition." Energy & Fuels 29.8 (2015): 5290–5302.

As Published: http://dx.doi.org/10.1021/acs.energyfuels.5b01040

Publisher: American Chemical Society (ACS)

Persistent URL: http://hdl.handle.net/1721.1/105463

Version: Author's final manuscript: final author's manuscript post peer review, without publisher's formatting or copy editing

Supercritical Water Treatment of Crude Oil and Hexylbenzene: An Experimental and Mechanistic Study on Alkylbenzene Decomposition

Adam G. Carr[1], Caleb A. Class[2], Lawrence Lai[2], Yuko Kida[2a], Tamba Monrose[2], William H. Green[2]

1 – Aerodyne Research Inc., 45 Manning Rd. Billerica, MA 01821
2 – Massachusetts Institute of Technology, 77 Massachusetts Avenue, Cambridge, MA 02139
a:- Present address - Dow Chemical Company, Freeport TX

Abstract

High concentrations of fuel-range hydrocarbons may be recovered from heavier alkyl-aromatic compounds in crude oil after supercritical water (SCW) treatment. Arabian Heavy (AH) crude oil was treated in SCW and analyzed using two-dimensional gas chromatography (GC×GC FID). Cracking mechanisms were investigated using the model compound hexylbenzene under similar SCW treatment conditions. The results of the model compound experiments were compared to predictions of a kinetic model built by the Reaction Mechanism Generator (RMG).

AH crude cracked significantly during SCW treatment. The GC-observable mass fraction increased by 90%. We conducted studies on the distilled samples of crude oil, and found that significant changes in the composition of the SCW-treated 'heavy' fraction occurred. Significant formation of aliphatic hydrocarbons and small-chain BTX-type compounds were found in the SCW-processed samples. Hexylbenzene conversions differed between the crude oil studies and the model compound studies. It is possible that hexylbenzene (and other alkylbenzene) conversion is hindered by preferential cracking of heavier hydrocarbons in the bulk crude oil solution.

The mechanistic model run for the cracking of hydrocarbons in SCW treatments of the model compound hexylbenzene resulted in the major liquid products toluene, styrene and ethylbenzene. The selectivity of ethylbenzene and styrene changed over time. The apparent conversion of styrene into ethyl benzene was possibly via a reverse disproportionation reaction. Ultimately a mechanism was built that serves as a basis for understanding the kinetics of hydrocarbon cracking in SCW.

Introduction

Supercritical water (SCW) is seen as an attractive upgrading and desulfurization medium for crude oil processing. SCW has unique properties that set it apart as an ideal solvent for organic reactions, including a low dielectric constant, high ion product and high diffusivity [1]. Industry has recently taken an active interest in using water as a reactive solvent, with patents approved for oil and bio-crude oil upgrading [2-5]. This is partly because there is published literature that has demonstrated that heavy hydrocarbons exposed to supercritical water produce significant concentrations of gas and light liquid products[5-8]. It has also been shown that water may enhance the production of benzene, toluene and xylene (BTX) compounds from crude oil in the presence of sulfur [9]. As such, it is conceivable that SCW could be used as a two-in-one unit

operation to both desulfurize crude oil [10, 11] and crack heavier hydrocarbons to light hydrocarbons, thus increasing the recovery of more valuable fuel-grade petroleum products.

Analysis on AH crude oil, AH crude oil fractions and reacted products is difficult, as there are well over 10,000 species present in crude oil. Two-dimensional gas chromatography (GC×GC) is a powerful tool, with methods that have been developed to analyze and detect crude oil components with aliphatic chains of up to about 25 carbons[12, 13]. GC×GC is a technique whereby two different chromatography columns connected in series with a modulator fractionate analytes via different mechanisms. For example, one column may separate analytes by molecular size, and the other by polarity. The system is highly tunable based on the mixture being separated and identified. Here we use GC×GC with a flame ionization detector (FID) to analyze the reactants and products from the supercritical water treatment of crude oil and crude oil fractions in order to quantify hydrocarbon species formed from the SCW treatment.

Previous work using a sulfur-sensitive detector has demonstrated that the amount of GC-observable material increases significantly when AH crude is treated with supercritical water. The implication of this result is that heavy compounds which are not volatile enough to pass through the GC crack to produce lighter aliphatic and aromatic hydrocarbons which are. The work presented in this paper builds on that work to demonstrate that not only is this apparent for those compounds containing sulfur, but it is also true for non-sulfur bearing hydrocarbons. As it is difficult to accurately quantify all species in the crude oil mixture, in this article we focus on the cracking of alkylated aromatic compounds with up to two aromatic rings. Furthermore, we elucidate some of the mechanisms involved in the SCW cracking of alkyl aromatic compounds by performing experiments using hexylbenzene as a model compound. We further compare the free radical mechanisms of those reactions performed in the water environment to a 'neat' pyrolysis environment.

Method

a) Reactor Method

The method for operating the batch reactor has been described in an earlier publication[14]. For the Arab Heavy (AH) crude oil and distillation fraction experiments, 1.0 g of AH crude oil was loaded with 3.5 g water in a 24 mL 316-stainless steel batch reactor built from SITEC fittings. The reactor was purged of air using helium (He). Post-purge, 20 bar of He was left in the headspace of the reactor to facilitate gas collection and quantification. We find leaving some gas in the reactor also avoids condensing droplets of fluid in the small-diameter tube at the top of the reactor leading to the pressure gauge. The sealed reactor was lowered into a 450 °C fluidized sand bath (Techne FB-05). After 5 minutes of operation, the pressure in the reactor stabilized, indicating the end of the warm up period. After 30 minutes, the reactor was quenched in a water bath. These conditions were selected based on a previous paper [10], where high conversions were obtained with model compounds. The organic phase was separated from the oil phase by pipetting the lighter organic phase from the top of the aqueous phase. The products were placed into pre-weighed collection vials, weighed and either directly analyzed using the GC-FID/GC×GC-FID directly, or after dilution in CS_2. For these samples, 3-chlorothiophene was used as an external

standard due to the isolated region in which this compound eluted relative to the other hydrocarbons.

For the model compound experiments, hexylbenzene was treated in SCW and without SCW. For the SCW experiments, a total of 4.8 mmol of hexylbenzene was loaded into the reactor with 3.5 g of water. Naphthalene was chosen as an inert internal standard due to its stability in SCW within the reaction time and temperature range of our experiments. Preliminary studies done without naphthalene present in the reactor with hexylbenzene in water showed no naphthalene was formed. The molar ratio of hexylbenzene to naphthalene in the feed was 10:1. Experiments carried out 'neat' (i.e. without water) used the same molar loading and molar ratio in the reactor as the experiments carried out in SCW. Samples were injected unfiltered into the GC-MS/FID and GC×GC-FID. A comparison between the filtered and unfiltered samples was done by diluting the obtained product in CS_2 and using a Whatman Anotop inorganic membrane syringe filter (0.02um) to remove and filter half of the obtained sample from the reactor.

b) Materials

AH crude oil was obtained from Saudi Aramco. The properties of AH crude are available in the published literature [15]. Hexylbenzene (analytical standard, ≥99.8%, Fluka) was used for the model compound studies, which was obtained from Sigma Aldrich. Deionized water was used for all experiments, as filtered through a Millipore unit with 18MΩ electrical resistance. All standards mentioned in other sections of this paper were obtained from Sigma Aldrich at the highest purity available. Gas phase standards were obtained from Airgas. Ultra high purity helium was obtained for Airgas for purging reactor headspace and as the carrier gas for GC.

c) Vacuum Distillation for Crude Oil Heavy and light Fractions

A simple vacuum distillation apparatus was used to separate light and heavy fractions of AH crude oil, as described previously but with an added packed column and pressure gauge [10]. A small flow of He was bubbled through the oil to prevent bumping. The vacuum was induced using a Pfeiffer vacuum pump. The pressure was controlled using an MKS pressure transducer and a user-operated HiP needle valve. Pressure was kept constant at 300 Torr ±5 Torr. The liquid distillate was collected in a flask immersed in ice water, and the gases emerging from that flask were passed through a trap immersed in liquid nitrogen. The distillation was halted when the temperature in the boiler reached 320°C. Both the 'distillate' fractions and the 'bottoms' fractions were collected and treated, and then used to compare GC×GC-FID results from both fractions with that of raw and treated crude oil.

d) GC-FID Method

Gas phase products were analyzed using a Shimadzu GC-2010 with a 5 μL sample-injection loop connected to a 30 m, 530 μm ID, 20 μm film thickness Rt-Q-Bond column and FID detector. The temperature program had an initial temperature held at 35 °C for 3 min followed by heating to 260 °C at 25 °C/min and held for 5 min. . The total number of moles of the gas formed was determined from the measured pressure pre-and post-experiment (the reactor volume is known).

The relative concentrations of the gases were measured against a custom calibration mixture of the expected vapor phase products, supplied by Airgas.

e) GC×GC FID Method

The main analytical tool for the crude oil experiments was the GC×GC-FID system (Leco). The primary column was an RXi-5HT, 30 m length, 250 μm ID, 0.25 μm film thickness. The secondary column (in a secondary oven held about 15°C above the temperature of the primary column) was an RXi-17SIL MS, 2 m length, 150μm ID, 0.15 μm film thickness. The modulation time was 5 seconds. The effluent from the GC is analyzed by FID. The injector was held at 300 °C. Known amounts of 3-chlorothiophene (3-CT) were spiked into the oil-phase product as a standard. 3-CT was chosen as it is not a constituent of crude oil, and it appears as a distinct peak in the chromatogram. The GC temperature ramp was from 50 °C to 320 °C in 90 min.

GC×GC-FID chromatograms were analyzed with GC image software (Zoex Corp), which integrates the signal in user chosen regions of the 2D signal trace. A peak volume is calculated from the obtained signal with a background signal subtracted.

Calibrations for the GCxGC FID were performed in thirteen concentrations with seventeen species, consisting of: pentane, hexane, octane, dodecane, tetradecane, hexadecane, benzene, toluene, ethylbenzene, propylbenzene, butylbenzene, hexylbenzene, octylbenzene, dodecylbenzene, naphthalene, 2-methylnaphthalene, and 1,2-dimethylnaphthalene. Compounds that could not be obtained for calibration purposes were quantified by extrapolating compound calibration curve slope values per 'carbon' of aliphatic chain length addition. The assumption for these species was that the response per additional 'CH2' group was linearly proportional to the signal outside of the range of those compounds that were calibrated. Similar assumptions were applied to the benzene groups. We also assumed that all of the signals were for saturated hydrocarbons. For example, ethyl naphthalene and vinyl naphthalene would have been the same species for quantification purposes.

The identification of compounds were done manually on crude oil; GC image subsequently uses this first identification as a template and applies this identification scheme to all other samples analyzed by GCxGC-FID in this study. The manual identification groups compounds and its close neighbors into the number of carbons and functional group it belongs to. The y-position of each streak of peaks allow identification between aliphatic (bottom streak), alkylbenzene (middle streak), and alkylnaphthalene (top streak), whereas the number of carbons were counted starting from the lightest species, with help from prior knowledge of certain species during calibration such as hexane, benzene, naphthalene, and other species listed as compounds used for calibration.

f) GC-FID/MS Method

The organic liquid phase products of the model compound experiments were analyzed using a GC-FID (Agilent 7890), using an RXi-5HT, 30 m length, 250 μm ID, 0.25 μm film thickness. The Aglient Mass Spectrometer was only used for identification purposes, while the FID was used to calibrate the organic liquid phase species. For the hexylbenzene studies, every quantified compound was calibrated in the GC-FID/MS (thus no peaks needed to be modeled for calibration quantification

purposes in the model compounds study). However, a few small peaks heavier than hexylbenzene were not quantified as discussed later.

g) RMG Mechanistic Modeling Method

The Reaction Mechanism Generator (RMG) was used to build kinetic mechanisms for this work [16]. The RMG algorithm has been discussed extensively in past work [17, 18], and only a brief introduction will be provided here. The most important feature is a flux-based algorithm for model generation, pursuing reaction pathways in directions with greater flux while omitting those with low predicted fluxes. RMG produces a file containing NASA polynomials to estimate thermochemical parameters for each of the species in the mechanism, as well as the modified Arrhenius parameters for each reaction. This file can be imported into CHEMKIN-PRO to simulate the kinetic experiments, and conduct flux and sensitivity analyzes [19].

For this work, mechanism generation and simulation conditions were chosen to match the experimental conditions as closely as possible. Mechanisms were generated in RMG using the experimental temperature, pressure, and starting concentrations (one with and one without SCW). Reactor simulations were conducted using the "Isothermal Closed Homogeneous Batch Reactor" model in CHEMKIN-PRO. The input decks used for the RMG and CHEMKIN-PRO simulations are given in the supporting information.

h) *Ab Initio* Calculations

Previously calculated Arrhenius and thermochemical parameters are available in literature for the decomposition mechanisms of alkylaromatic [20] compounds, and some of these were added to the RMG database to assist in parameter estimation for this work. In addition, the RMG database is able to estimate reasonably accurate rate parameters for many other relevant reactions using previously calculated data. However, when generating mechanisms containing thousands of reactions, it is not possible to find extremely accurate rate parameters for each of the predicted reactions. Thus, some of them must be roughly estimated, and these estimations can be uncertain by multiple orders of magnitude. These uncertainties are mitigated by calculating more accurate rate coefficients using *ab initio* techniques. Ab initio rate coefficient calculations can still be uncertain by up to a factor of ten, so it is important to consider these uncertainties when analyzing these reaction mechanisms.

In this work, some reactions were identified as having a significant effect on the rate of phenyldodecane decomposition, and the initially estimated parameters were improved using quantum mechanics and transition state theory. Gaussian 03 [21] was used to determine the geometries and vibrational frequencies of stable molecules and reaction transition states at the B3LYP/6-311G(2d,p) level of theory, and single point energies were calculated using CBS-QB3. Barrier heights for particularly important reactions, including the retroene reaction depicted in Figure 1, were refined using CCSD(T)-F12a/cc-pVDZ-F12 single point energies, which have been proven to have improved accuracy [22-24]. These coupled-cluster calculations were conducted using Molpro [25].

The open-source CanTherm [26] software package was used to calculate rate constants and thermochemical parameters using transition state theory. A scaling factor of 0.99 was used for the frequency analysis. One-dimensional hindered rotations were also included in this analysis, using dihedral angle scans at the B3LYP/6-311G(2d,p) level of theory in 10 degree increments, performing constrained optimizations at each point. The effective moment of inertia $I^{(2,3)}$ was calculated for each hindered rotor. Modified Arrhenius constants were then derived for each of these reactions, and these parameters were added to the RMG database to improve model generation.

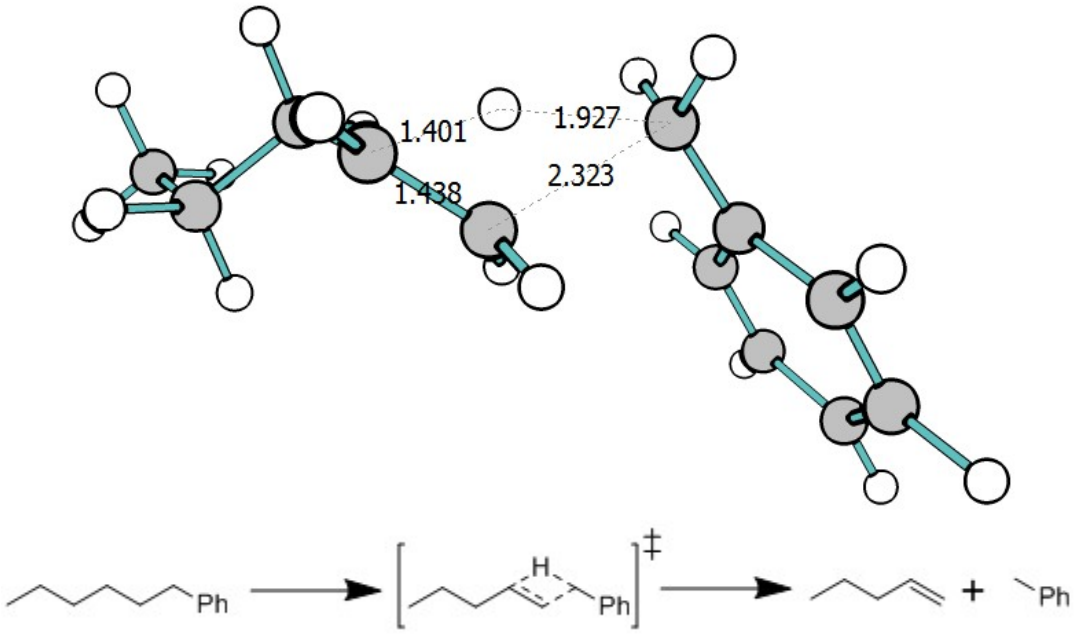

Figure 1. Transition state geometry (top) for retroene reaction to produce toluene and 1-pentene (bottom). Interatomic distances in Ångstrom.

Results and Discussion

a) GC×GC FID crude oil treatment in SCW

AH crude oil was treated and analyzed in the GCxGC-FID. In this study, the three classes of species were studied: aliphatic compounds, alkyl benzenes, and alkyl naphthalenes. These species represented the bulk of GC×GC observable hydrocarbons. The combined observed mass fractions of each of these three classes for each of the analyses performed are shown in Table 1.

The GC×GC FID chromatogram of crude oil (with standard) is shown in Figure 2a. Only 34% of the mass is observable by GC. The majority of the species present in crude oil could not be observed due to their high molecular weights and therefore low volatility as can be seen by the heavy skew of the obtained GC×GC chromatogram towards the heavy components. The heaviest compound that was detected by the GC×GC was $C_{32}H_{66}$, which has a boiling point of 467°C [10]; higher molecular weight compounds injected into the GCxGC do not reach the detector. The compounds that had higher boiling points remain in the GC inlet as liquids, and solidify when cooled. This was

evident by observing the GC×GC inlet liner, which had visible unvolatilized crude oil still present post-injection.

The raw crude oil was treated in SCW, and in a control experiment under a purged, inert helium atmosphere (pyrolysis). Typical pressures of the SCW experiments were 330bars (gauge). Under non-SCW conditions, pressures were typically 75 bars (gauge). The variation in pressure between runs for both SCW and pyrolysis conditions was within 7% of the average pressure value. The results of the GC×GC -FID analysis of the raw and treated samples are shown in Figure 2a, b and c. The total observable mass fraction in the GC×GC -FID after SCW treatment increased from 34% to 65%, which corresponded to a net 90% increase in the GC-observable compounds. This is indicative of the fact that heavier components cracked to produce lighter hydrocarbons, which thus became detectable in the GC×GC. This is further supported by the physical appearance of the product being much less viscous than the reactant crude oil.

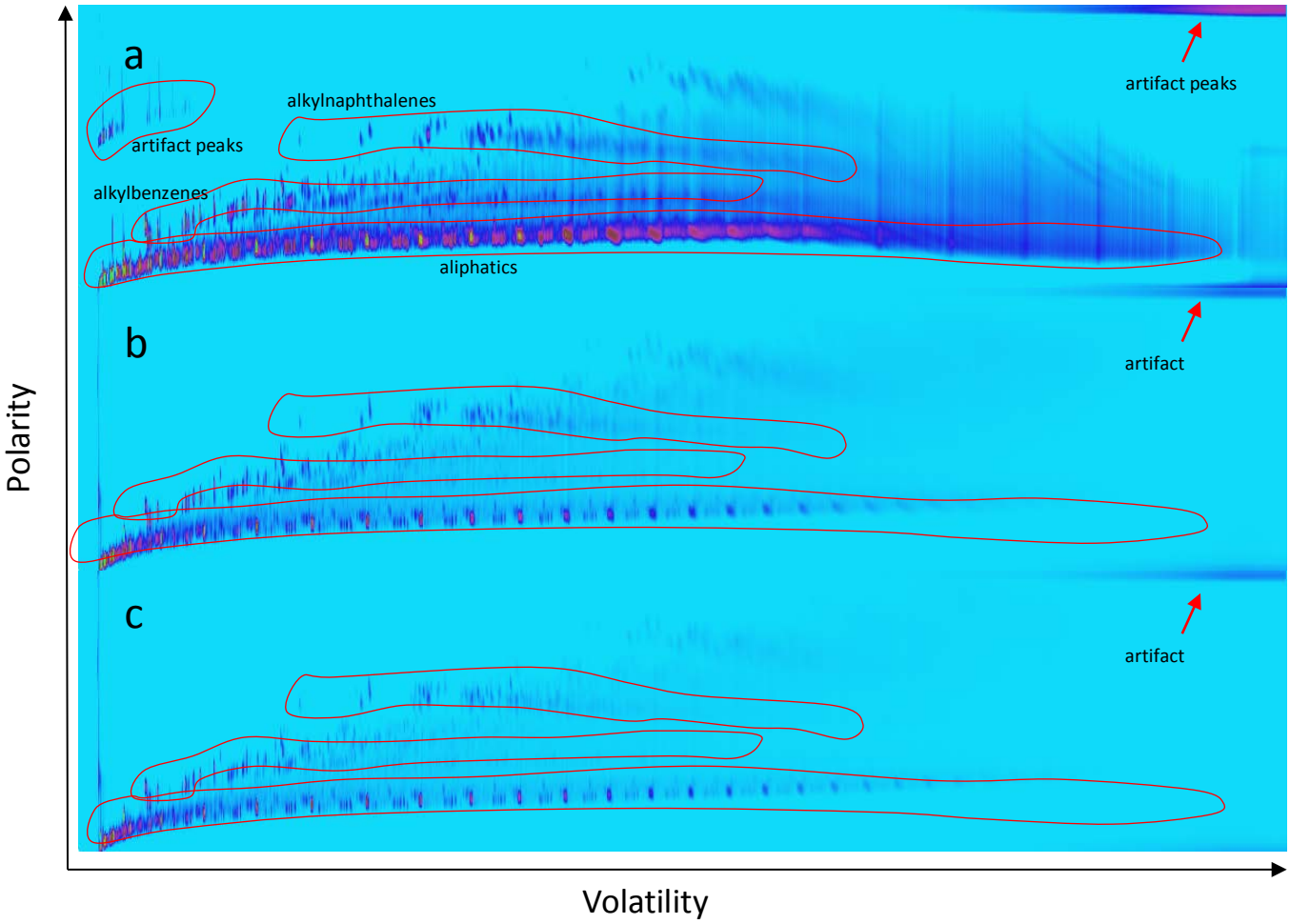

Figure 2: GCxGC-FID chromatograms of a) Raw Arabian Heavy Crude Oil and b) SCW Treated Arabian Heavy Crude Oil, and c) Pyrolysis Treated Arabian Heavy Crude Oil

Table 1: Total GC-observed mass fractions for various samples and species. Most of the hydrocarbons were too heavy to be observed in the GC×GC chromatogram. The 'Total' column is the ratio of the sum of calibrated peak mass (in each of the columns to the left of the total column) for each compound observed in the GC as compared to the mass, as measured by gravimetry. The raw calibrated mass distribution is shown in the *Supporting Information Section S2.* Pyrolysis treated bottoms products results are not presented, due to the heavy fouling of the reactor that occurred when attempting the experiment

	Aliphatics	Alkylbenzenes	Alkylnaphthalenes	Total
Raw Crude Oil	15%	7%	12%	34%
Raw, SCW Treated	28%	17%	20%	65%
Raw, Pyrolysis Treated	25%	12%	16%	54%
Distillate	48%	24%	8%	80%
Distillate, SCW Treated	39%	26%	8%	73%
Distillate, Pyrolysis Treated	42%	22%	7%	71%
Bottoms	3%	3%	14%	20%
Bottoms, SCW Treated	14%	4%	14%	35%

The product distribution of the compounds that eluted from the GC×GC is shown in Figure 3. The compounds are classified into functional groups, followed by the number of carbons on the branch of the aliphatic group. For example, ethyl benzene and xylene are both classified as alkylbenzenes with two carbons (C2), and n-butane and isobutene are both classified as aliphatics with four carbons (C4). Thus each carbon number represents every isomer of the carbon chain. Similarly, unsaturated aliphatics are lumped with saturated aliphatics. The volume of each contour under the 2D images are processed through the "GC Image" software and calibrated using the external standard.

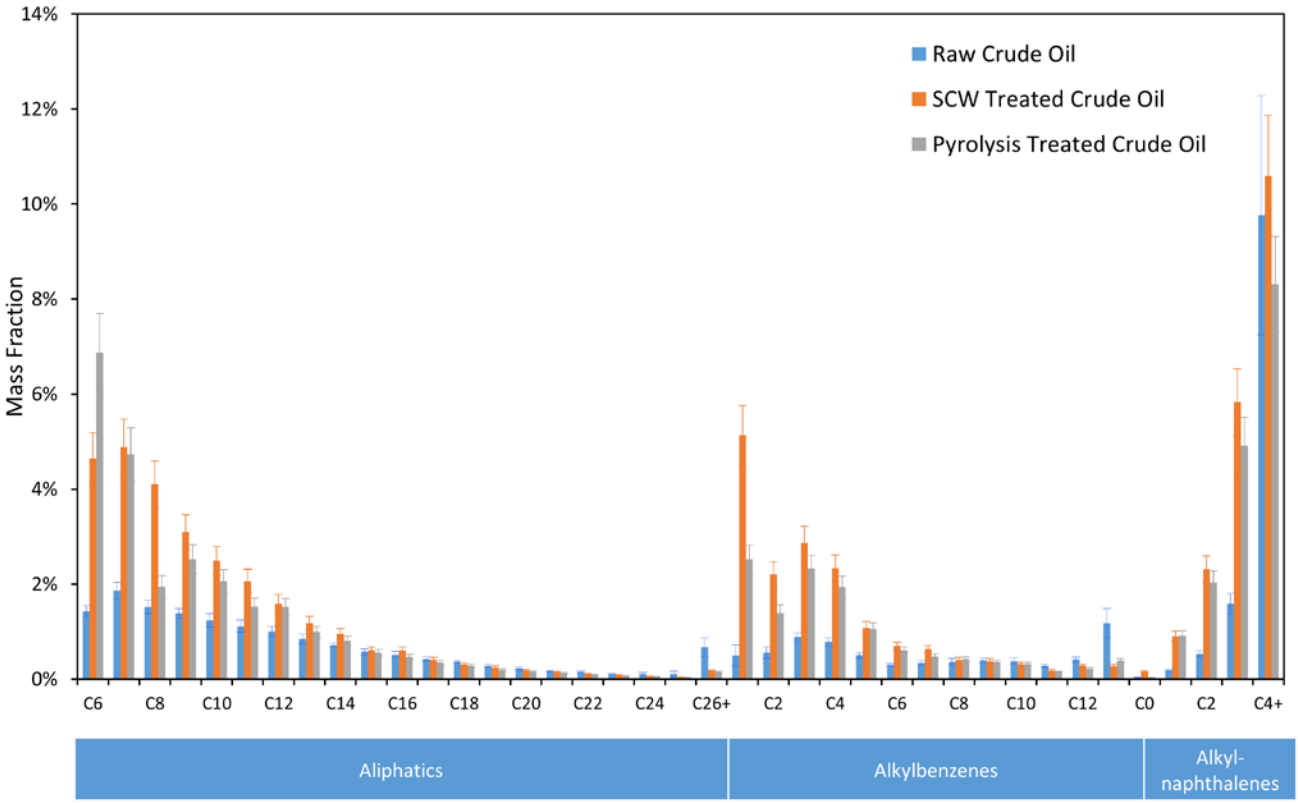

Figure 3: Observable mass fraction of crude components pre- and post-treatment. Note that the sum of the peaks will not reach 100% due to the unobservable mass fractions, as corroborated in Table 1. Error bars were produced by repeated measurements. Note the increase of C6-C9 aliphatics, and decrease in C10+ alkylbenzenes, indicating the cracking of oil components.

The SCW and pyrolytic treatment of crude oil resulted in a significant increase in relative weights of lighter components (such as C6-C10 aliphatics, C1-C5 alkylbenzenes and C1-C3 alkylnapthalenes). Similarly, heavier aliphatics (C26+), alkylbenzenes (C9+) and alkylnaphthalenes (C4+) had a significant decrease. The general increase in light products is indicative of the cracking of the heavier oil components. Similarly, the increase of C2 and C3 alkylnapthalene concentration may have come from the cracking of higher molecular weight species. This is investigated in the treatment of crude oil fractions section of this paper.

Toluene had the largest relative increase in concentration; sixfold over what was observed in the raw crude oil. This is typical of beta scission in alkylated aromatics under similar environments, as observed in the model compound studies shown later in this paper. C2 and C3 alkylnaphthalenes also exhibited a similar increase, which is indicative of a similar mechanism. The higher concentration of product C2 and C3 alkylnaphthalenes, as opposed C1 alkylnaphthalenes, is likely the result of a higher concentration of multiply branched isomers of alkylnaphthalenes than with alkylbenzenes.

There were slight differences between the product distributions obtained after AH crude was treated by pyrolysis and by SCW treatment. Approximately 50% more C6 aliphatic hydrocarbons

were formed in the pyrolysis case than in the water case. Conversely, there was 40% less toluene in the products in the pyrolysis case than in the water case.

Similarly, more branched aromatics were obtained in the SCW-treated case. These branched aromatics may have come from heavier components of the crude oil that contained aromatic rings, as the balance of formed branched polycyclic aromatic species could not be closed from the observed C13+ alkylbenzenes and/or C4+ alkylnaphthalenes in the raw crude oil. Furthermore in all cases studied in this paper, a higher mass recovery was obtained when crude oil was treated with SCW, indicating that the increase in mass is likely to have originated from the unobservable hydrocarbon fractions.

b) Treatment of Crude Oil Fractions

In order to examine on which fractions the SCW and pyrolysis treatments had the most effect experiments were conducted on vacuum-distilled products of AH crude oil. The GC×GC-FID chromatogram of the distilled and 'bottoms' fraction is shown in Figure 4a and Figure 5a. The cut between the fractions was reasonably sharp, showing very little overlap of individual fractions. SCW treatment was performed on both of these fractions, and the results are shown in Figure 4b and Figure 5b. The pyrolysis treated distillate fraction is shown in Figure 4c.

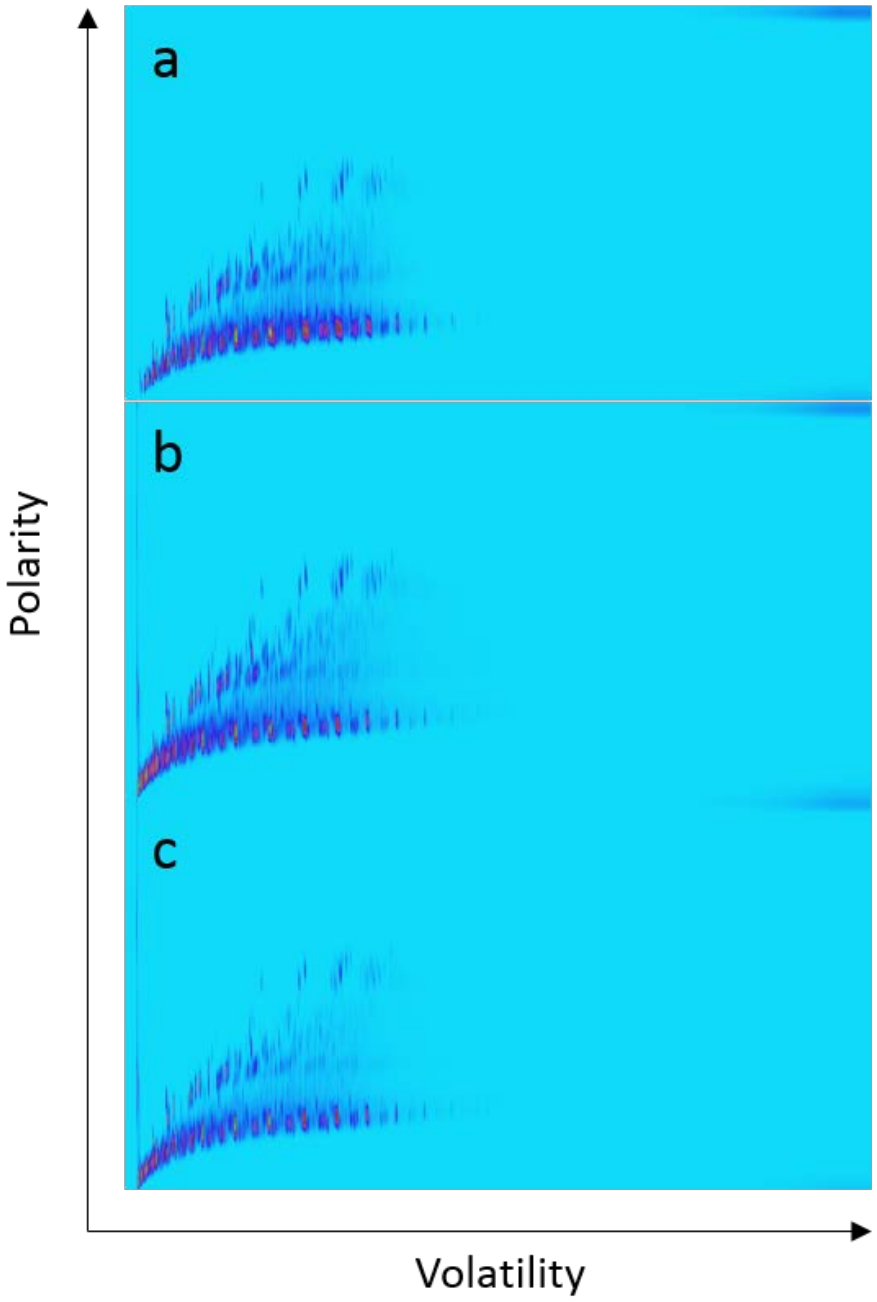

Figure 4: GCxGC-FID Chromatogram of the a) distillate fraction, b) SCW treated distillate and c) Pyrolyzed distillate. The SCW or pyrolysis treatment alters the composition only subtly

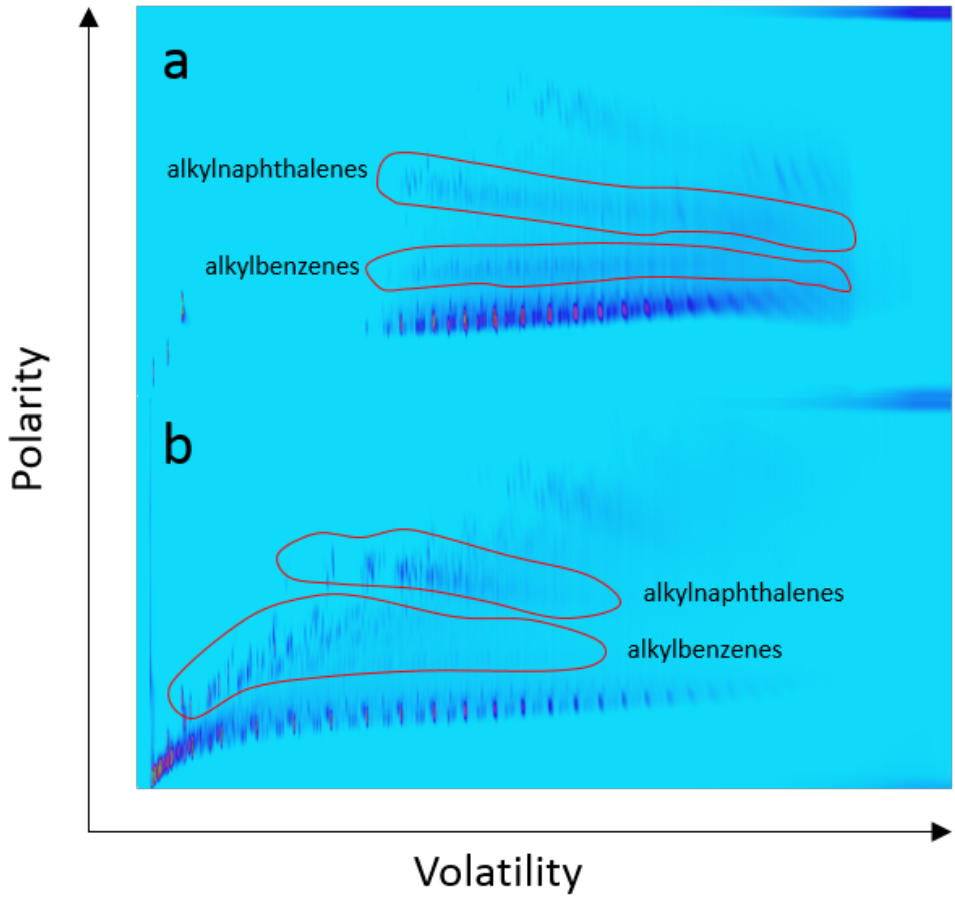

Figure 5: GCxGC-FID chromatograms of the a) bottoms fraction, and b) SCW treated bottoms of Arabian Heavy Crude. SCW or pyrolysis treatment of the bottoms fraction drastically changes the composition

The quantified product distribution observed in the raw and SCW treated bottoms fraction is shown in Figure 6.

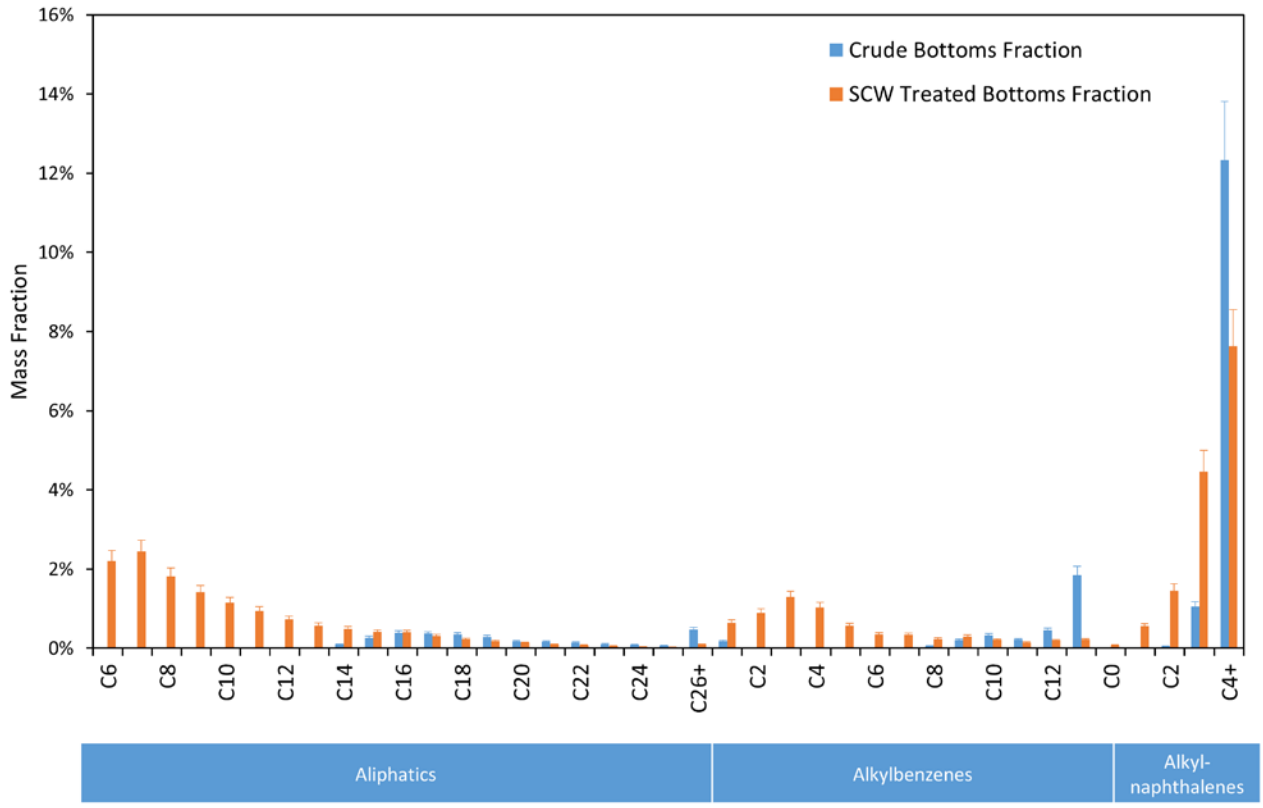

Figure 6: Mass fractions of crude bottoms components pre- and post-treatment. Note that the sum of the peaks will not reach 100% due to the unobservable mass fractions, as corroborated in Table 1.

SCW treatment of the bottoms product significantly changed its composition. The overall observable mass in the GC×GC increased by 75%, as shown in Table 1. High concentrations of C6-C14 aliphatic hydrocarbons were formed from heavier material. Similarly, C1 to C8 alkylbenzenes and significant quantities of C0-C3 alkylnaphthalenes were formed by SCW treatment.

The bottoms fraction experienced a dramatic decrease in the concentration of alkyl benzenes of twelve carbons and higher, which is consistent with the observations for the SCW-treated whole crude oil case. Similarly, it appears the C4+ alkylnaphthalenes crack to form C3, C2 etc. alkylnaphthalenes.

The results of the treated distillate fraction experiments are shown in Figure 7. Very little difference was observed between the SCW- and pyrolysis-treated distillate samples. However, the yield of alkylbenzenes was measured to be 15% higher in SCW than in the pyrolysis case, which is slightly higher than the experimental error. The lower yield of the pyrolysis-treated crude sample may be due to the formation of components that are lighter than observable in the GC×GC which in these experiments only measured species with 6 to 32 carbon atoms. However, the product size distribution of the pyrolysis case does not indicate any greater formation of lighter components by mass fraction than the SCW case (the bulk of the 'light' aliphatics are normally distributed around C10, similar to the SCW case Conversely, it may be possible that pyrolysis forms chars that are also unobservable in the GC×GC. The latter explanation is consistent with results on the model

compounds, which will be described later in this paper. While the products are unfiltered when injected in the GC×GC, we do not observe significant solid phase products prior to injection into the GC×GC. These observations are consistent with results on the model compounds, which will be described later in this paper.

There was a slight shift in the mass distribution for the aliphatic hydrocarbons post-SCW and pyrolysis treatment. The local maximum concentration of aliphatic carbons shifted from C10 to C8. The change was minimal, however it indicates that a small amount of cracking occurs to smaller molecular weight aliphatic species present in the distillate solution.

The relative distribution of alkylbenzene and alkylnaphthalene products did not appear to shift significantly. Without heavier fractions present to generate the radicals necessary for cracking, fewer radicals were present in the solution. This would correspondingly reduce the overall reactivity [10]. However, for alkylbenzenes we observed hydrocarbons with alkyl branches of C6+ had a lower net yield in the product distribution, whereas C5- alkyl branches increased relative to the raw distillate product. As an increase of C6+ alkylbenzenes was observed in the raw crude treatment, it is clear that the additional C6+ benzenes were being formed from the cracking of higher molecular weight compounds in the non-GC observable species in AH crude oil.

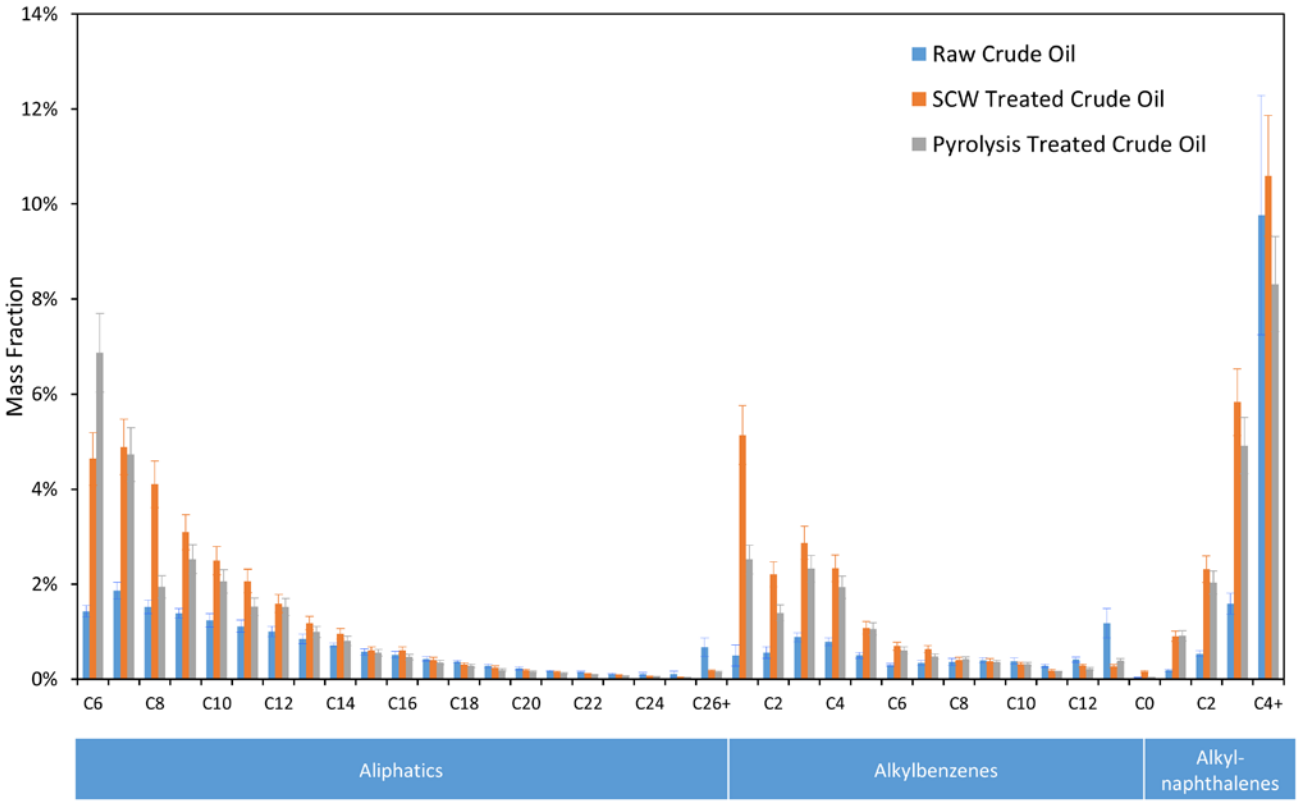

Figure 7: mass fraction of crude distillate components pre- and post-treatment. Note that the sum of the peaks will not reach 100% due to the unobservable mass fractions, as corroborated in Table 1. Error bars were produced by repeated measurements.

c) Alkylbenzene treatment in SCW

In order to investigate the mechanisms for crude oil cracking in SCW, hexylbenzene was treated in SCW and in pyrolysis conditions. Hexylbenzene was treated both with and without SCW at 450°C for 3 different residence times. The pressure of the reactor with water present was 338 bars ± 4%. The pressure in the 'neat' pyrolysis cases was 74bars ±18%. The variation in the final pressure during the reaction was mostly due to the thermal expansion of water and helium from pre-reaction conditions.

The conversion of hexylbenzene in water and without water is shown in Table 2. In both SCW and pyrolysis cases, the conversion was nearly complete (93%) at 40mins residence time. Overall conversion was the similar in both water and pyrolysis cases, within experimental uncertainty.

Table 2: Conversion of hexylbenzene

	SCW			*Pyrolysis*		
	15min	30min	40min	15min	30min	40min
Conversion	0.41	0.83	0.91	0.46	0.80	0.93

The liquid-phase products of the hexyl benzene experiments are shown in Figure 8. The trends are consistent with cracking of similar compounds in the literature [26]. The highest concentration product in the liquid phase was toluene, followed by ethylbenzene, propylbenzene and styrene. This is similar to the results obtained in the cracking of raw and distilled crude oil, shown earlier in this paper.

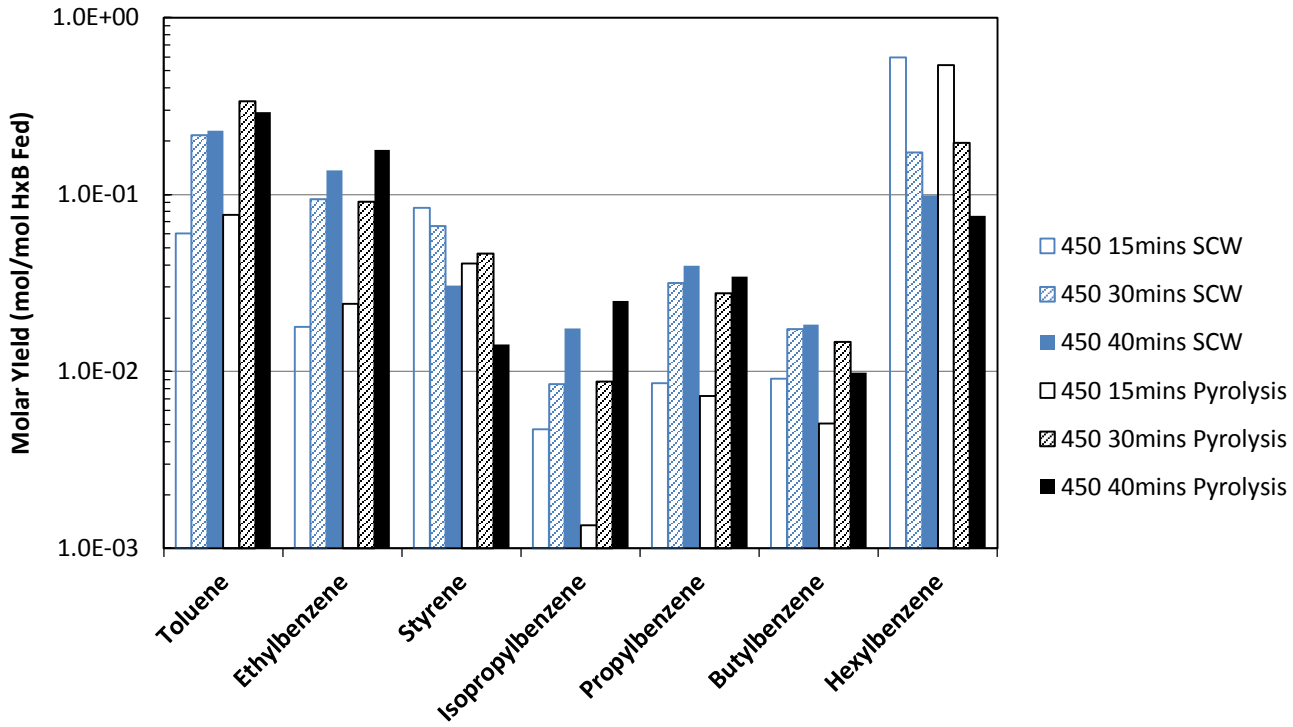

Figure 8: Molar yield of liquid (organic phase) products

Styrene was present in higher concentrations at lower residence times than ethylbenzene for both SCW and pyrolysis treated cases. However, at longer residence times the concentration of ethylbenzene was higher than styrene. It is likely that styrene slowly reacts to form ethylbenzene, possibly via reverse-disproportionation reactions that were previously investigated [19]. However, the final yield of ethylbenzene is two to three times higher than the peak yield of styrene, suggesting there may be other routes to ethylbenzene.

All of the observed compound concentrations were similar with water and without water across all residence times. No CO or CO_2 was detected post-reaction using NDIR spectrometry, so it is unlikely that the water reacted directly with the hydrocarbons.

The gas phase product concentration distribution is shown in Figure 2. The dominant gas phase products by mole fraction basis were n-butane and ethane. The butane corresponds to the major liquid co-product styrene.

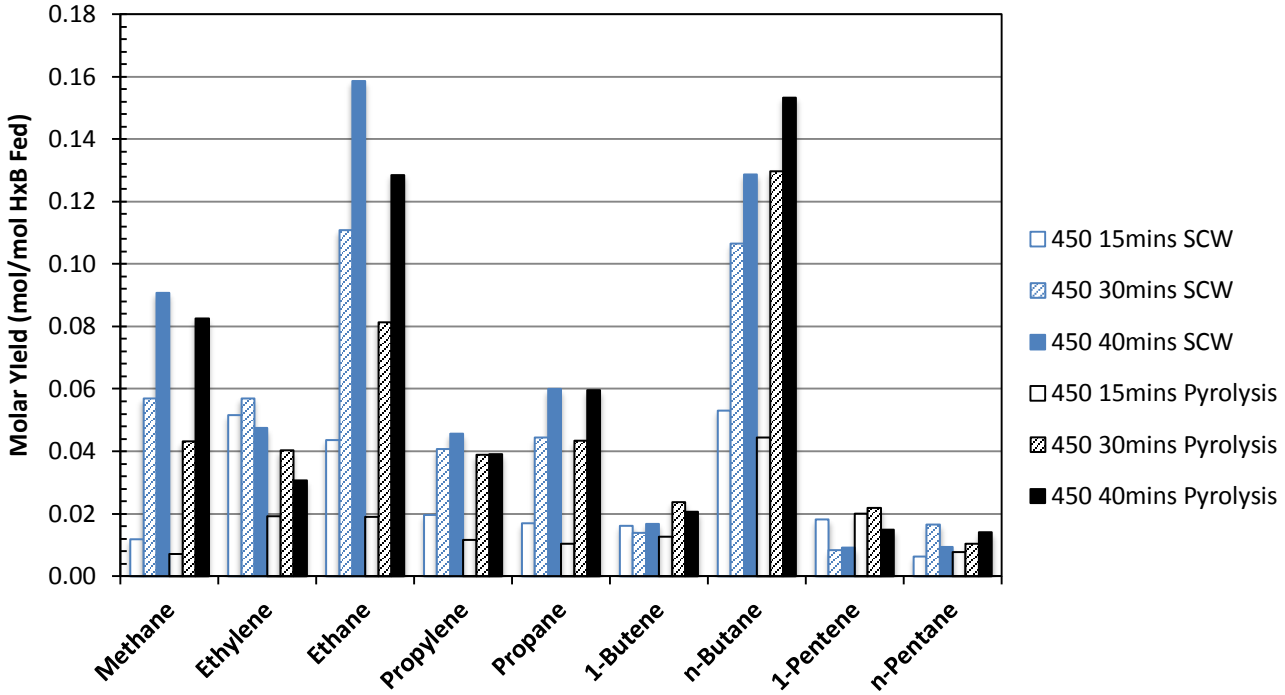

Figure 9: Molar yield of gas-phase product distribution post water- and pyrolysis treatment –

The expected relative yields of vapor phase products did not directly correspond to the products observed in the liquid/organic phase in the longer residence time experiments. For example, toluene was the highest concentration product in the organic phase, therefore the expected products of hexylbenzene cracking where toluene was a product in the gas phase should be 1-pentene. The fact that this was not the case indicates that the initial products, such as 1-pentene, would have further reacted and formed smaller products, such as propylene, ethane, butadiene and methane. Clearly fragmentation occurred, as small vapor phase products existed in lower relative concentrations in the 15 min runs (for both water and without water) while significantly increasing at residence times above 30mins, as shown in Figure 2. Similarly, pentene yield decreased at higher residence times in the hexylbenzene studies, as shown in Figure 9.

Based on the recovery of the internal standard, each experiment performed had a near-complete mass recovery in the liquid phase. A benzene balance showed a 77% ± 7% of the benzene was recovered in the experiments performed. It is possible that some of the carbon formed larger molecular weight products outside of the detection range of the GCs. A few small peaks are observed with retention times larger than hexylbenzene, as shown in Figure 10. While this does not conclusively demonstrate that the carbon loss was not due to the formation of high molecular weight species it may still be possible. Similar observations have been made in a previously published paper [10], which shows that the observed mass loss is not unique to this study.

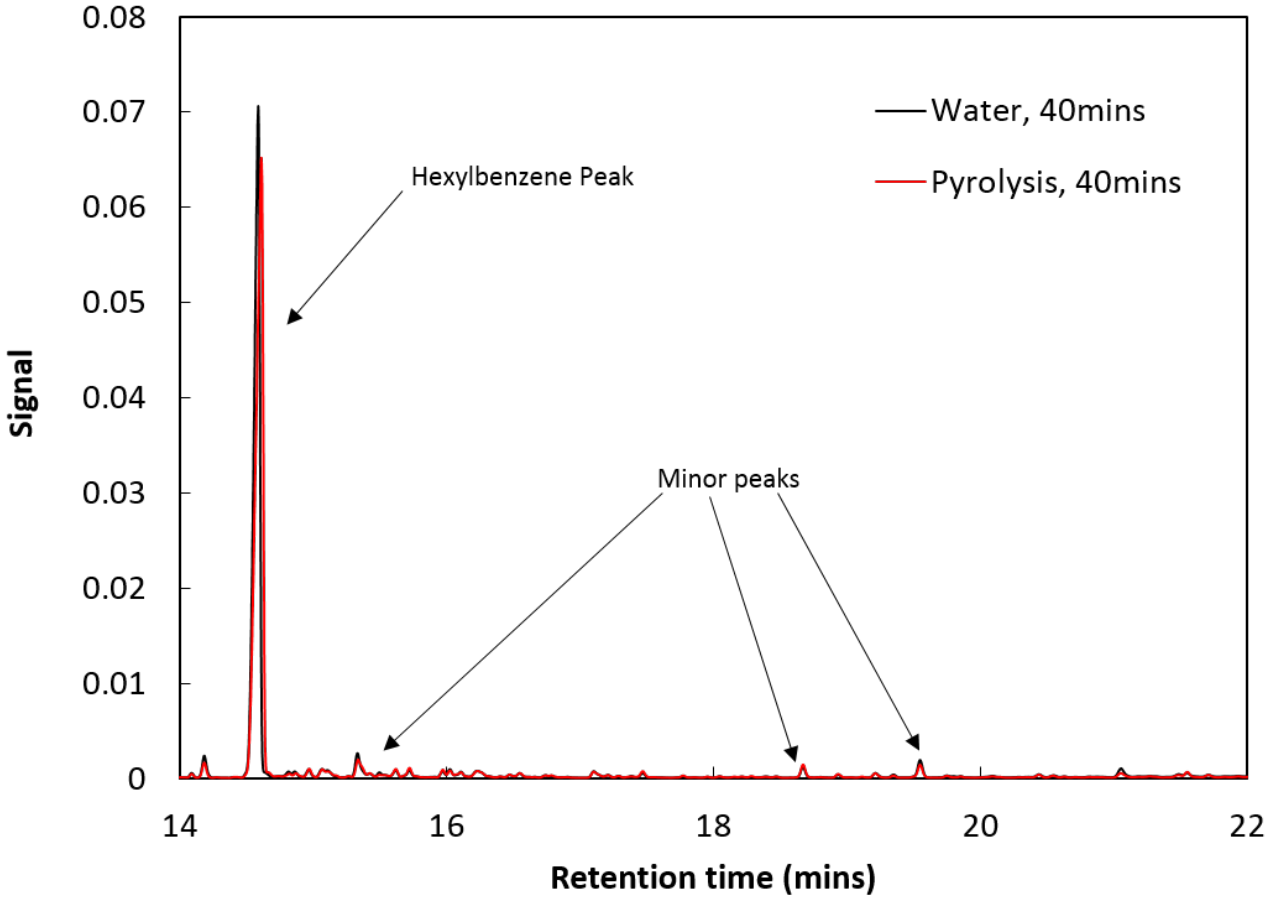

Figure 10: "Tail-end" chromatogram showing low concentrations of GC-FID detectable species with higher molecular weight than hexylbenzene. The signal on the y-axis is the ratio of the observed peak signal to that of the internal standard naphthalene

Further visual observation of reactor products from both the pyrolysis and water studies showed a very small amount of black powder-like material. While the products were observable visually, quantifying the amount by weight was not possible because amount of material observed was negligibly low. Filtration of the products recovered from the Hexylbenzene study through a 0.02µm hydrophobic syringe filter resulted in an unchanged product distribution when injected through the GC-MS/FID and GC×GC-FID, as shown in Figure 11. Similarly, upon cleaning the reactors from the pyrolysis studies, small black specks were visible, though only in the pyrolysis studies. However, the amount of solid recovered from cleaning was so small that quantification was not possible. It is likely that the black material is not have been in the detectable range of the chromatography techniques, however as the benzene balance was high, it is likely that the mass in the solid phase was negligible.

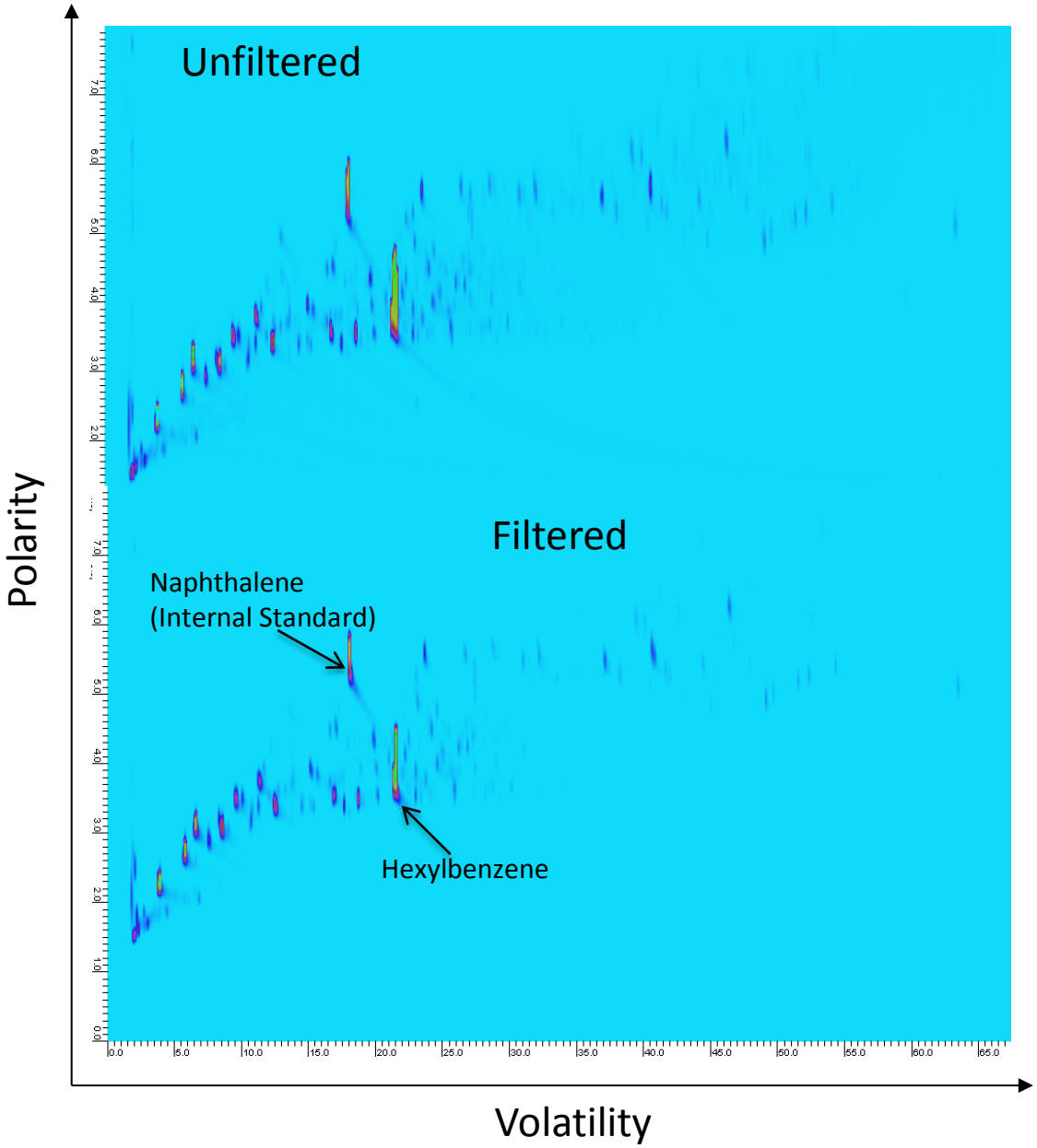

Figure 11: GC×GC-FID chromatogram of the filtered and unfiltered product distribution from SCW treatment of hexylbenzene at 450°C, 30 mins. The major products are more volatile than hexylbenzene, but many species less volatile than hexylbenzene are also formed.

Some multicyclic aromatic species were identified by GC×GC performed on the SCW and pyrolysis products using the same method as for the crude oil studies, as shown and discussed in the Supporting Information section *S1*. Streaks in the two-ring alkylaromatic region were observed. However, the observed peaks were small relative to the major products observed. Relative to the naphthalene standard, the largest peak was about 6% by volume. This corresponds to the relative area observed in the GC-FID shown in Figure 10. The additional observed molar mass (of all previously unquantified aromatic species) was about 7%, thus increasing the mass balance to 99% (in the 40 min pyrolysis case). However, the lower residence time experiments did not show

significant formation of multi-ringed aromatics, and no increase in the mass balance was observed. The SCW-treated case at 40min residence time had a mass balance increase of 6%, which was lower than for the pyrolysis case. This was expected, as it has been shown in the published literature that the concentration of aromatic species is lower in SCW cases than in non SCW cases [7]. It also is consistent with the observation of a darker color product in the pyrolysis case than in the SCW case, as shown in Figure 12.

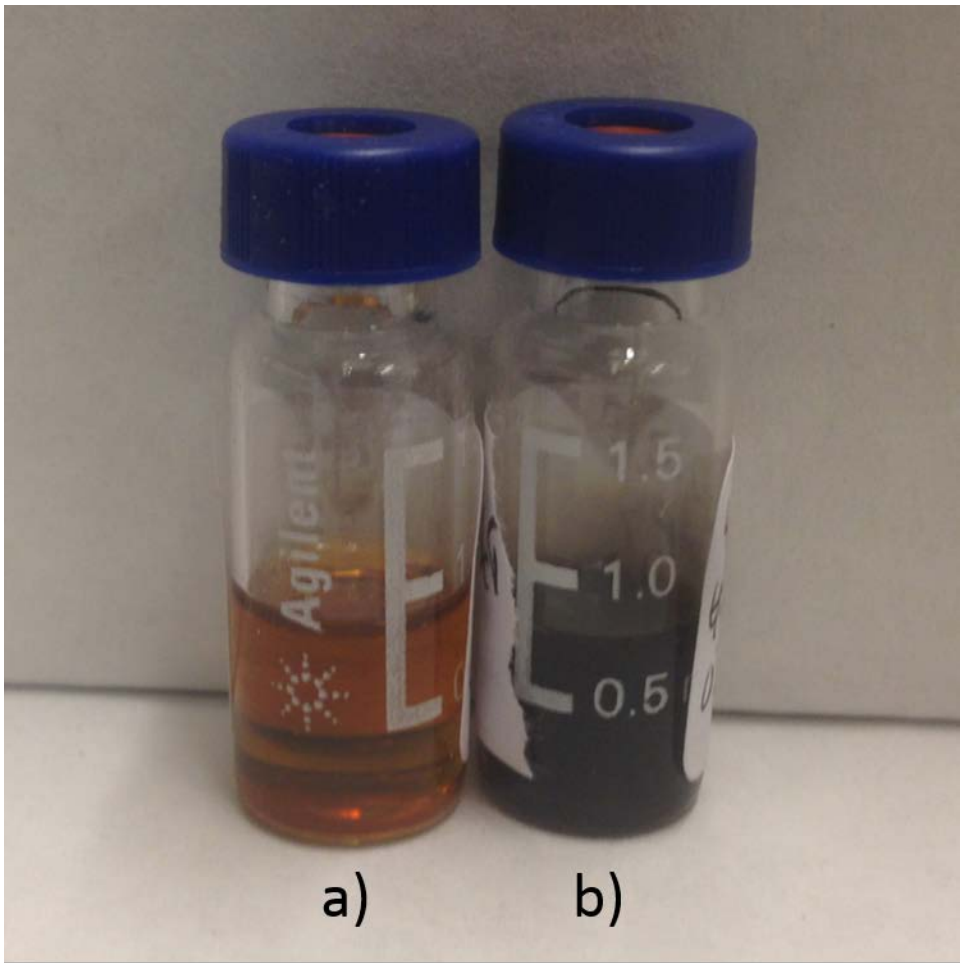

Figure 12 Color of the organic phase produced from hexyl benzene after 40 mins at 450C a) SCW treatment and b) pyrolysis treatment.

The product distribution in the organic liquid phase was similar to other aromatic hydrocarbon pyrolysis results available in the published literature carried out in similar conditions, as shown in Table 3. While the single aromatic ring species predominantly formed toluene in our work and that of Savage et al. [27], dodecylpyrene produced significant concentrations of pyrene and the corresponding C_{12} alkene. In the present experiment, we did not observe any significant concentration of benzene or hexane. The benzene we did observe was a factor of ten below what was observed by [27], despite having reached a higher conversion. Thus our observations do not support the conclusion that the occurrence of aryl alkyl bond cleavage is independent of the number of aromatic rings as speculated in [28]. However, it may be the case that where there are

fused aromatic rings the occurrence of alkyl-aryl bond cleavage is universally more important, and more similar between different species.

Table 3: Table comparing pyrolysed products in this work with those under similar conditions in the literature

Alkylbenzene Products/Liquid Phase
Molar Yield (corrected for 6 highest concentration products)

Reference ->	This Work	This Work	[27]	[29]
Compound	hexylbenzene	hexylbenzene + Water	dodecylbenzene	dodecylpyrene
T	450	450	400	425
P (Bar)	67	334	-	-
time	40	40	240	60
ArCH3	0.41	0.51	0.455	0.157
ArC2H5	0.21	0.27	0.121	0.048
ArC2H4	0.047	0.022	0.006	0.000
ArC3H8	0.053	0.046	0.024	0.015
ArC4H10	0.022	0.012	0.027	0.000
Unreacted	0.099	0.076	0.357	0.182
Pyrene				0.598
Benzene	0.001	0.001	0.011	

The observed conversion of C6-substituted benzenes in the crude oil experiments was significantly lower than the conversion of hexylbenzene in the model compound studies. Indeed, the concentration of C6-substituted benzenes increased in cases where the heavy crude oil fraction was present, as shown in Table 4. Alkylated aromatics are clearly generated from the cracking of heavier hydrocarbons. As most of the 'bottoms' fraction compounds were outside the detectable range, we are not able to identify which bottoms compounds crack to form the C6-substituted benzenes.

Table 4: Weight Percent of C6-substituted benzenes measured in the crude oil and model compound experiments.

Feed	C6-substituted benzenes in the Feed (wt %)	C6-substituted benzenes in the organic phase product of SCW treatment (wt %)	C6-substituted benzenes in Pyrolysis products (wt %)
Raw Crude	0.32	0.7	0.6
'Bottoms' Fraction	0	0.354	N/A
Distillate Fraction	1.9	1.6	1.6
Hexyl Benzene	100	9	7

The formation of C6-substituted benzenes in the Crude and especially the Bottoms experiments is certainly due to cracking of high molecular weight molecules. However, it is less clear what is happening in the Distillate experiment, where the feed does not contain much material heavier than C6-substitute benzenes. In the Distillate experiment, the C6-substituted benzene concentration dropped by only 17%; contrast that with >90% conversion of the hexyl benzene in the pure model compound experiment. The main apparent difference between the Distillate and Hexyl Benzene model-compound experiments is the concentration of alkyl aromatics; we examine the effect of higher hexylbenzene product concentration on the conversion of hexylbenzene in the modeling section of this paper.

c) Mechanistic Modeling Results

The reaction mechanism generated to model the pyrolysis experiment contains 137 species and 1706 reactions, while the SCW model contains 129 species and 1697 reactions. The CHEMKIN input files and RMG species dictionaries for these mechanisms have been included in the Supporting Information. The major reaction pathways predicted for the two cases are effectively identical, in agreement with the experimental results. The main reaction steps, including fluxes, are presented in Figure 13. Hexylbenzene pyrolysis is predicted to proceed mainly via normal cracking, in accordance with previous modeling research on alkyl aromatics [20]. The "retroene reaction," the molecular reaction forming pentene and toluene from the reactants, is predicted to provide appreciable toluene production, although only about 10% of the overall decomposition was via this pathway. This is in agreement with previous studies, which predicted 80% of toluene production via this molecular pathway at 330 °C, but only 20% at 400 °C [26]. However, while toluene is observed as a major product in the experiments, 1-pentene, which is produced in both the free radical and molecular pathway, is observed in much smaller amounts. One possible pathway accounting for this was predicted by RMG, and it is presented in Figure 14. Hydrogen abstraction from 1-pentene leads to formation of a resonance stabilized radical, which breaks off a methyl group to form 1,3-butadiene. This diene is predicted to undergo Diels Alder with another unsaturated compound to form a cyclic alkene, which could undergo further Diels Alder reactions to produce fused cyclic species. This pathway is predicted to consume over half of the produced 1-pentene, and the Diels Alder reaction would consume other unsaturated species, as well.

Styrene is predicted as a major product via beta-scission pathway. Experimental results from this and previous work [19] suggest that this compound is an intermediate in the formation of

ethylbenzene, although our experiments at 450 °C show some styrene remaining as a product after 40 minutes. RMG predicts that the reverse disproportionation pathway leads to some production of ethylbenzene, but this reaction is less dominant than at lower temperatures.

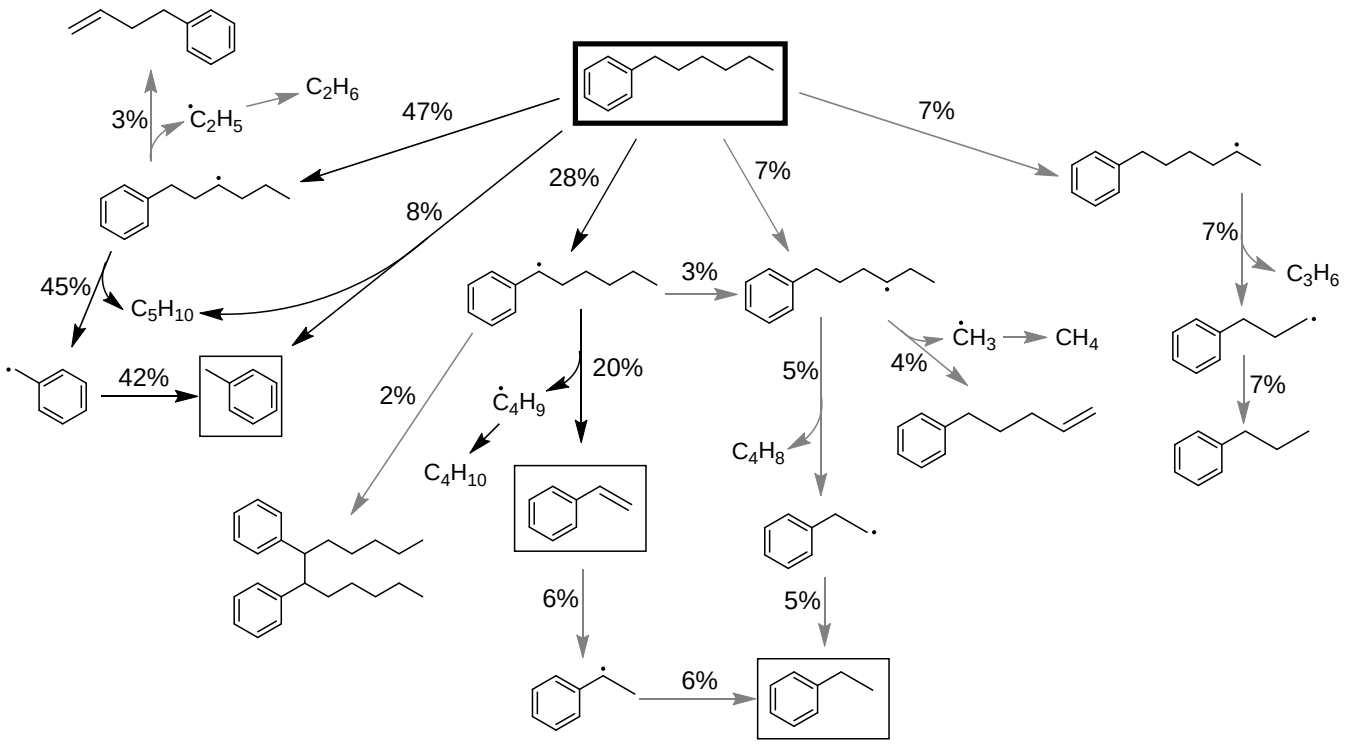

Figure 13. Primary reaction fluxes for the pyrolysis of hexylbenzene at 450 °C. Fluxes presented as percentage of overall decomposed hexylbenzene proceeding through a given pathway, with most reactions below 3% omitted for clarity.

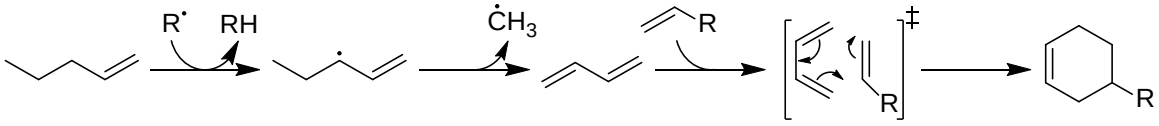

Figure 14. Secondary decomposition and Diels Alder addition pathway for 1-pentene and other alkenes.

A comparison of experimental vs. model predictions is plotted in Figure 15 for hexylbenzene conversion, Figure 16 for the main aromatic products, and Figure 17 for the light products. Reasonable agreement is observed for the reactant conversion, suggesting that the rate constants and thermochemistry for the main reaction steps are reasonably accurate. Mechanisms with and without water predict identical rates of hexylbenzene conversion, which agrees with experimental measurements. Toluene is well predicted, but 1-pentene is overpredicted by a factor of three, suggesting that other secondary consumption pathways, which were not predicted by RMG, are also possible. Most other light products are predicted within a factor of two. This is within the modeling uncertainty, and it is also important to note the uncertainty in the experimental quantification, which is significantly more difficult in the case of gas phase products.

The sum of ethylbenzene and styrene production predicted by RMG reasonably agrees with what was observed experimentally, which also suggests that the first few reaction steps are predicted well. However, ethylbenzene is underpredicted by the model while styrene is significantly overpredicted, likely due to two factors. First, the expected reverse disproportionation pathway,

which seems to be supported by the experimental results, has been predicted to be slower than necessary to account for the observed amount of ethylbenzene. This disagreement is likely due to the uncertainty in the calculation of rate constants for disproportionation reactions, which is about a factor of 10. Second, RMG predicts a number of large molecules (two or more benzene rings) to be produced from these experiments, and each of these compounds is predicted in very small amounts. The low concentration of each of these species is reasonable, as there are many different possible radical addition, recombination, and Diels Alder products; no single large compound is likely to be produced in great quantity. On the other hand, we propose that many different large molecules are produced in these experiments, each in rather small quantities. This hypothesis is supported by the small peaks observed on the heavier end of the GC chromatographs, as well as the lack of benzene balance closure, which is also observed for hexyl thiophene. The production of large molecules is expected to proceed more quickly in the absence of water based on the experimental results, as a darker product was observed when water was not present in the reaction mixture. Improved modeling of these larger species is an important topic of future work.

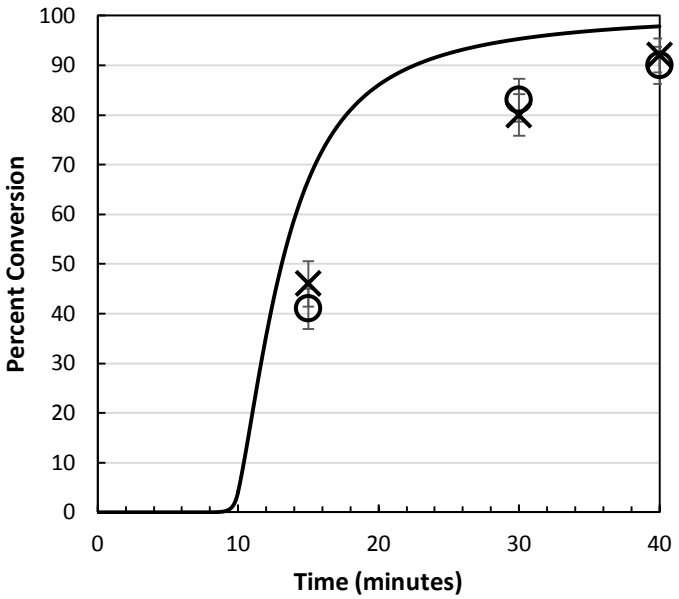

Figure 15. Hexylbenzene conversion vs. time at 450 °C. (x) pyrolysis experiment, (o) SCW experiment, (—) model predictions. Pyrolysis model and SCW model predictions precisely overlap.

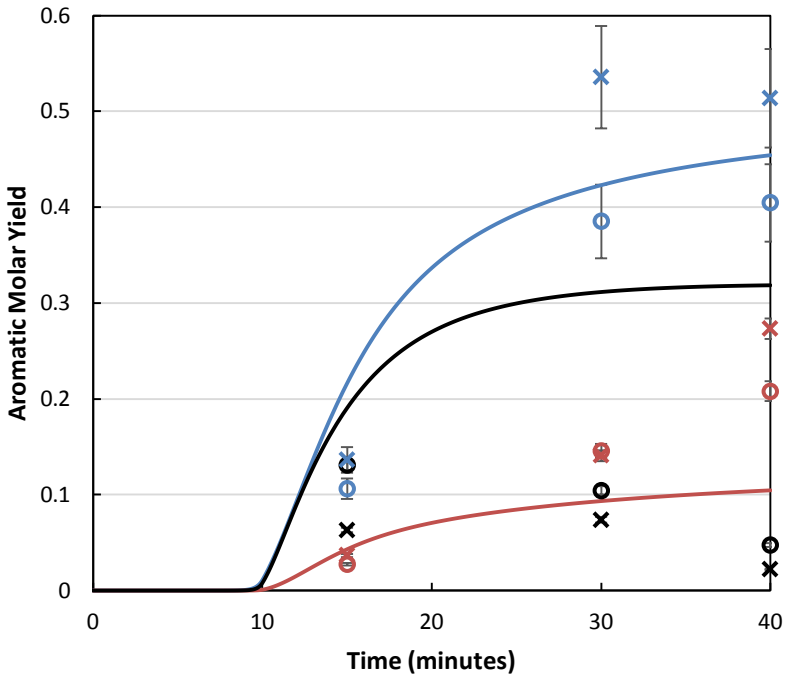

Figure 16. Model (solid lines) comparison with experiments (pyrolysis x, SCW o) for production of toluene (blue), styrene (black), and ethylbenzene (red). Aromatic molar yield is defined here as fraction of total aromatic compounds present as the given product.

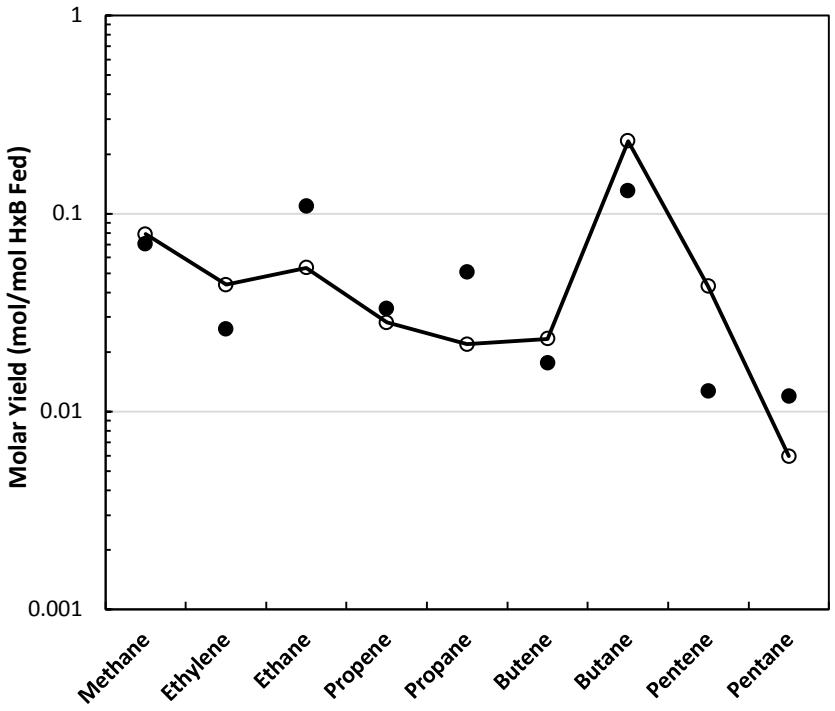

Figure 17. Predicted (o, solid line) and observed (●) light products after pyrolysis treatment for 40 min at 450 °C

C6-substituted benzenes are not as reactive in the SCW-treated Distillate study as hexylbenzene is in the model compound study. A simulation was conducted to examine the effect of dilution by

alkanes (in the simulations, by pentane) on hexylbenzene conversion in supercritical water. The mechanism was run with equal initial concentrations of pentane and hexylbenzene, and also with ten times as much pentane as hexylbenzene. The computed molar yields of cases with different amounts of pentane are shown in Figure 18. These calculations show that dilution in alkanes only slightly affects alkylaromatic conversion and product distributions (i.e. the alkanes are mostly inert at this temperature, as might have been expected).

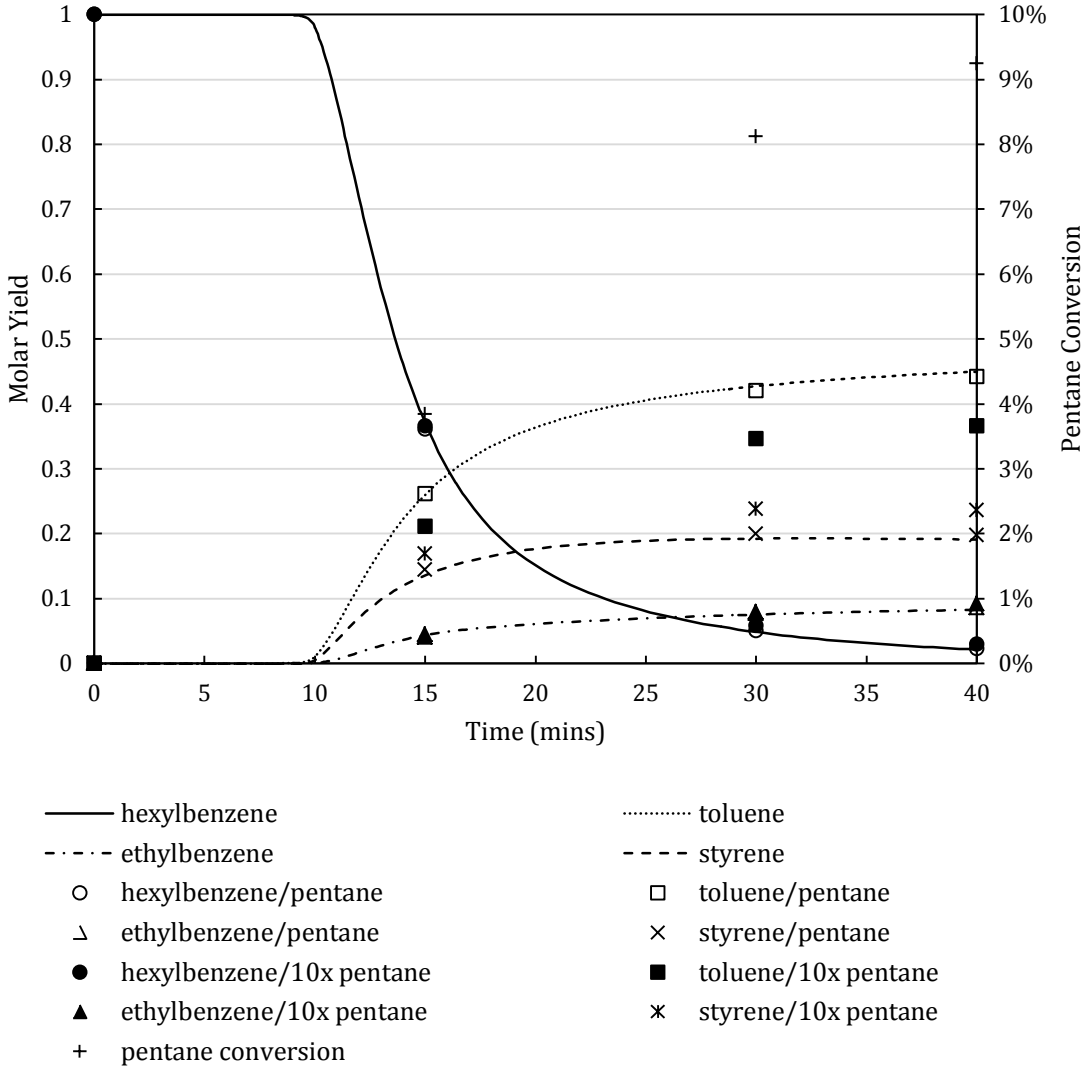

Figure 18: RMG-predicted product distribution comparison of hexylbenzene treatment in SCW with and without additional pentane (1:1 and 1:10 by mole). It was hypothesized that higher dilution of alkyl aromatic would result in lower conversion, thus possibly explaining why hexylbenzene conversions were different in the crude oil and model compound cases. Based on the mechanism constructed in RMG, this does not appear to be the case.

Conclusions

Supercritical water treatment of crude oil resulted in the recovery of over 75% more fuel-grade hydrocarbons. Branched aromatic hydrocarbons were cleaved during supercritical water

treatment of crude oil, as analyzed by GC×GC FID. It has been shown that the formation of smaller branched hydrocarbons is the result of cracking hydrocarbons that are heavier than what is discernable in the GC×GC FID chromatograms. The cleavage of aliphatic hydrocarbon chains from aromatic rings predominantly occurs via beta scission in the alkane chain. The major products toluene and ethylbenzene primarily form through this route. Molecular kinetic modeling in RMG accurately predicts the conversion of hexylbenzene, and most of the major product concentrations are predicted within the margin of error of the model. However, the concentration of styrene is overpredicted in the model at each conversion point measured in the reactor. In the model, styrene is consumed in a reverse disproportionation reaction, but the predicted rate is too slow to explain the experimental observations. The model also does not predict all the minor products observed. While water appears to play some role in the recovery of a higher amount of carbon in the cracking reactions, and it strongly affects the color of the products even in model compound experiments, the mechanism by which this occurs is yet to be determined.

Acknowledgements

The authors gratefully acknowledge the support of Saudi Aramco for funding this study under Contract Number 6600023444. We also acknowledge Dr. K.-H. Choi for helpful conversations.

Supporting Information Available

Full kinetic models in CHEMKIN format for pyrolysis and supercritical water treatment of hexylbenzene in CHEMKIN format, with comments on the source of each reaction's rate parameters, and a corresponding dictionary of structures in RMG format (readable using the GUI at http://rmg.mit.edu) and additional detailed information from the experimental product analyses. This information is available free of charge via the internet at http://pubs.acs.org/.

Cited References

1. Carr, A.G., R. Mammucari, and N.R. Foster, *A Review Of Subcritical Water As A Solvent And Its Utilisation For The Processing Of Hydrophobic Organic Compounds.* Chemical Engineering Journal, 2011. **172**(1): p. 1-17.
2. Choi, K.H., *Supercritical Water Process to Upgrade Petroleum*, US Patent 8,864,978, October 21, 2014
3. Gregoli, A., F. Leder, and U.M. Oko, *Process For Converting Heavy Crudes, Tars, And Bitumens To Lighter Products In The Presence Of Brine At Supercritical Conditions*, US Patent 4818370, April 4, 1989
4. Li, L., *Method Of Converting Triglycerides To Biofuels*, US Patent 7691159, March 20, 2010
5. Paspek Jr, S.C., *Upgrading Heavy Hydrocarbons With Supercritical Water And Light Olefins*, US Patent 4483761, November 20, 1984
6. Cheng, Z.-M., et al., *Effects of Supercritical Water in Vacuum Residue Upgrading.* Energy & Fuels, 2009. **23**(6): p. 3178-3183.
7. Moriya, T. and H. Enomoto, *Characteristics Of Polyethylene Cracking In Supercritical Water Compared To Thermal Cracking.* Polymer Degradation And Stability, 1999. **65**(3): p. 373-386.

8. Yang, M.-G., I. Nakamura, and K. Fujimoto, *Hydro-Thermal Cracking Of Heavy Oils And Its Model Compound.* Catalysis Today, 1998. **43**(3–4): p. 273-280.
9. Yang, Y., S.B. Hawthorne, and D.J. Miller, *Class-Selective Extraction of Polar, Moderately Polar, and Nonpolar Organics from Hydrocarbon Wastes Using Subcritical Water.* Environmental Science & Technology, 1997. **31**(2): p. 430-437.
10. Kida, Y., A.G. Carr, and W.H. Green, *Cleavage of Side Chains on Thiophenic Compounds by Supercritical Water Treatment of Crude Oil Quantified by Two-Dimensional Gas Chromatography with Sulfur Chemiluminescence Detection.* Energy & Fuels, 2014. **28**(10): p. 6589-6595.
11. Patwardhan, P.R., et al., *Supercritical Water Desulfurization of Organic Sulfides Is Consistent with Free-Radical Kinetics.* Energy & Fuels, 2013. **27**(10): p. 6108-6117.
12. Schoenmakers, P.J., et al., *Comparison Of Comprehensive Two-Dimensional Gas Chromatography And Gas Chromatography–Mass Spectrometry For The Characterization Of Complex Hydrocarbon Mixtures.* Journal of Chromatography A, 2000. **892**(1): p. 29-46.
13. Seeley, J.V. and S.K. Seeley, *Multidimensional Gas Chromatography: Fundamental Advances And New Applications.* Analytical chemistry, 2012. **85**(2): p. 557-578.
14. Kida, Y., et al., *Combining Experiment And Theory To Elucidate The Role Of Supercritical Water In Sulfide Decomposition.* Physical Chemistry Chemical Physics, 2014. **16**(20): p. 9220-9228.
15. Stratiev, D., et al., *Evaluation Of Crude Oil Quality.* Petroleum & Coal, 2010. **52**(1): p. 35-43.
16. Green, W.H., et al., *Reaction Mechanism Generator (RMG)*, 2013. http://rmg.mit.edu/
17. Allen, J.W., C.F. Goldsmith, and W.H. Green, *Automatic Estimation of Pressure-Dependent Rate Coefficients*, Physical Chemistry Chemical Physics, 2012. **14**. 1131-1155
18. Harper, M.R., et al., *Comprehensive Reaction Mechanism For N-Butanol Pyrolysis And Combustion.* Combustion & Flame, 2011. **158**(1): p. 16-41.
19. *CHEMKIN-Pro*, 2011, Reaction Design Inc.: San Diego.
20. Burkle´-Vitzthum, V., et al., *Mechanistic Modeling of the Thermal Cracking of Decylbenzene. Application to the Prediction of Its Thermal Stability at Geological Temperatures.* Industrial & Engineering Chemistry Research, 2003. **42**: p. 5791-5808.
21. Frisch, M.J., et al., *Gaussian 03*, 2004, Gaussian, Inc.: Wallingford CT.
22. Aguilera-Iparraguirre, J., et al., *Accurate Ab Initio Computation Of Thermochemical Data For C3Hx (X=0,...,4) Species.* Chemical Physics, 2008. **346**(1-3): p. 56-68.
23. Aguilera-Iparraguirre, J., et al., *Accurate Benchmark Calculation Of The Reaction Barrier Height For Hydrogen Abstraction By The Hydroperoxyl Radical From Methane. Implications For C(n)H(2n+2) where n = 2 -> 4.* Journal of Physical Chemistry A, 2008. **112**(30): p. 7047-7054.
24. Klopper, W., et al., *Accurate Coupled Cluster Calculations Of The Reaction Barrier Heights Of Two CH3 Center Dot + CH4 Reactions.* Journal of Physical Chemistry A, 2009. **113**(43): p. 11679-11684.
25. Werner, H.-J., et al., *Molpro: A General-Purpose Quantum Chemistry Program Package.* Wiley Interdisciplinary Reviews: Computational Molecular Science, 2011. **2**(2): p. 242-253.
26. Sharma, S., M.R. Harper, and W.H. Green, *Cantherm Open-Source Software Package*, 2010. http://rmg.mit.edu/
27. Savage, P.E. and M.T. Klein, *Discrimination Between Molecular And Free-Radical Models Of 1-Phenyldodecane Pyrolysis.* Industrial & Engineering Chemistry Research, 1987. **26**(2): p. 374-376.

28. Smith, C.M. and P.E. Savage, *Reactions Of Polycyclic Alkylaromatics. 1. Pathways, Kinetics, And Mechanisms For 1-Dodecylpyrene Pyrolysis.* Industrial & Engineering Chemistry Research, 1991. **30**(2): p. 331-339.
29. Savage, P.E., G.E. Jacobs, and M. Javanmardian, *Autocatalysis And Aryl-Alkyl Bond Cleavage In 1-Dodecylpyrene Pyrolysis.* Industrial & Engineering Chemistry Research, 1989. **28**(6): p. 645-654.

Supporting information for manuscript entitled:

Supercritical Water Treatment of Crude Oil and Hexylbenzene: An Experimental and Mechanistic Study on Alkylbenzene Decomposition

S1: GC×GC analysis of the Liquid Organic Phase Products

Analysis by GC×GC-FID was conducted to observe whether some multi-ringed aromatic species could be observed that did not appear in the GC-FID. The GC×GC method was identical to the method used for the crude oil analysis. The results are shown in Figure S1 for the 450°C, 40min pyrolysis case (which would have the highest theoretical multi-ringed aromatic compound formation of all experiments). While the alkylnaphthalene peaks appear in a relatively high concentration here, the product distribution is not representative due to the high volatility of the other liquid phase products (styrene, toluene, benzene, etc.). The loss of the smaller products here was largely due to the long shelf-time the products were exposed to after being extracted from the SCW reactor and before being run through the GC×GC-FID.

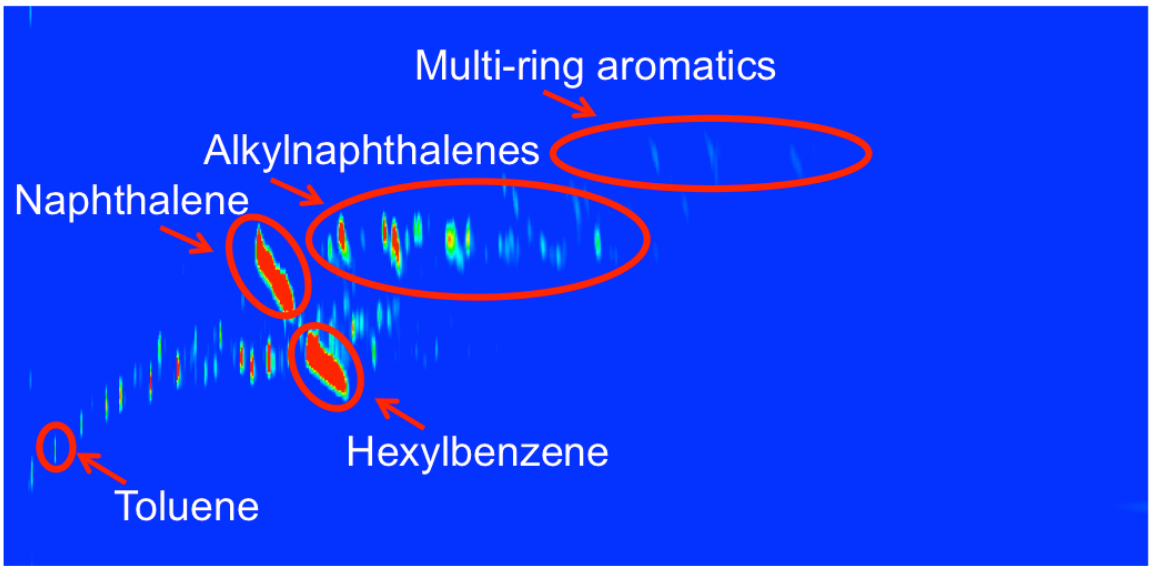

Figure S1: GC×GC-FID chromatogram of pyrolysis-processed products (450C, 40mins) of hexylbenzene.

A rough estimate of the total molar mass contained within the alkylnaphthalenes was obtained by multiplying the relative chromatogram peak volumes by the molar mass of the internal standard naphthalene. A table of the results for the results shown in Figure S1 is shown in Table S1. The estimated number of moles was 7% of the total mass observed in the GC-FID chromatograph, which brings the accounted for mass balance to 97%. This may be a high number, as naphthalene will have a higher volatility than the branched naphthalene compounds.

A similar increase in overall mass balance yield was found for the water case, as shown in Table S2. For the lower residence time experiments, no significant

formation of multi-ringed aromatics were identified, for both SCW and pyrolysis cases. Thus the mass balance for lower residence time experiments did not increase.

Table S1: Peak volume of the target analyte relative to naphthalene and the corresponding moles of the multi-ringed isomers for the pyrolysis experiments. The number suffix denotes the isomer. The number in the parentheses for the mass balance row indicates the change in total mass balance.

	Pyrolysis			
	450°C, 15mins		450°C, 40mins	
Peak Assignment	V/V% (naphthalene)	Moles	V/V% (naphthalene)	Moles
1Carbon Naphthalene	0.05%	2.46E-07	6.2%	3.04E-05
2Carbon Naphthalene	0.04%	1.90E-07	1.2%	5.64E-06
2Carbon Naphthalene2			5.4%	2.63E-05
2Carbon Naphthalene3			0.1%	3.91E-07
2Carbon Naphthalene4			0.2%	1.15E-06
3Carbon Naphthalene	0.03%	1.32E-07	0.8%	3.84E-06
3Carbon Naphthalene2			0.8%	4.13E-06
3Carbon Naphthalene3			0.3%	1.57E-06
3Carbon Naphthalene4			0.0%	5.56E-08
Total		5.69E-07		7.34E-05
Mass Balance post-PAH		62% (+0%)		96% (+7%)

Table S2: Peak volume analyte relative to naphthalene and the corresponding moles of the multi-ringed isomers for the supercritical water experiments. The number suffix denotes the isomer. The number in the parentheses for the mass balance row indicates the change in total mass balance.

	SCW			
	450°C, 15mins		450°C, 40mins	
Peak Assignment	V/V(naphthalene)	Moles	V/V(naphthalene)	Moles
1Carbon Naphthalene	0.007%	3.53E-08	0%	1.81E-06
2Carbon Naphthalene	0.035%	1.73E-07	2%	8.61E-06
2Carbon Naphthalene2			2%	8.03E-06
2Carbon Naphthalene3			3%	1.44E-05
2Carbon Naphthalene4			3%	1.62E-05
3Carbon Naphthalene	0.023%	1.11E-07	1%	7.21E-06
3Carbon Naphthalene2			0%	1.27E-06
3Carbon Naphthalene3			0%	3.54E-07
3Carbon Naphthalene4			2%	8.20E-06
Total		3.19E-07		6.61E-05
Mass Balance post-PAH		62% (+0%)		86% (+7%)

S2: Raw results of the GC×GC-FID chromatograms for crude oil

Table S3: Raw results of g/g product distribution as obtained by the GCxGC FID.

		Weight Fraction							
		Calibrated g of peak/total g weighed							
Group Name	*Name*	Crude Oil Raw	Crude Oil Distillate	Crude Oil Bottoms	SCW Treated Raw	SCW Treated Distillate	SCW Treated Bottoms	Pyro Treated Crude	Pyro Treated Distillate
Alkanes	*C6*	1.43E-02	7.68E-04	0	4.64E-02	3.76E-02	2.21E-02	6.87E-02	3.52E-02
	C7	1.86E-02	2.69E-02	0	4.89E-02	5.02E-02	2.44E-02	4.73E-02	4.55E-02
	C8	1.52E-02	5.63E-02	0	4.10E-02	6.51E-02	1.82E-02	1.95E-02	6.15E-02
	C9	1.39E-02	7.47E-02	0	3.09E-02	6.19E-02	1.42E-02	2.53E-02	6.30E-02
	C10	1.24E-02	7.66E-02	0	2.49E-02	5.32E-02	1.15E-02	2.06E-02	5.75E-02
	C11	1.12E-02	7.12E-02	0	2.07E-02	4.38E-02	9.44E-03	1.52E-02	4.93E-02
	C12	1.01E-02	6.53E-02	0	1.59E-02	3.41E-02	7.24E-03	1.52E-02	4.16E-02
	C13	8.46E-03	5.24E-02	3.67E-05	1.18E-02	2.29E-02	5.73E-03	9.94E-03	2.99E-02
	C14	7.19E-03	3.68E-02	9.67E-04	9.55E-03	1.45E-02	4.87E-03	8.04E-03	2.04E-02
	C15	5.77E-03	1.41E-02	2.72E-03	6.09E-03	5.87E-03	4.16E-03	5.57E-03	7.93E-03
	C16	5.15E-03	4.25E-03	3.95E-03	6.09E-03	1.92E-03	4.04E-03	4.66E-03	2.62E-03
	C17	4.26E-03	1.10E-03	3.69E-03	4.11E-03	4.49E-04	3.09E-03	3.52E-03	7.45E-04
	C18	3.66E-03	3.73E-04	3.48E-03	3.06E-03	1.49E-04	2.33E-03	2.81E-03	2.70E-04
	C19	2.83E-03	9.37E-05	2.92E-03	2.46E-03	8.66E-05	1.87E-03	1.94E-03	1.15E-04
	C20	2.30E-03	3.22E-05	1.77E-03	1.87E-03	0	1.39E-03	1.56E-03	3.03E-05
	C21	1.69E-03	1.25E-05	1.67E-03	1.44E-03	0	1.02E-03	1.20E-03	0
	C22	1.46E-03	8.33E-06	1.40E-03	1.08E-03	0	7.92E-04	8.65E-04	0
	C23	1.12E-03	0	1.04E-03	7.83E-04	0	5.72E-04	6.46E-04	0
	C24	1.05E-03	0	8.48E-04	5.82E-04	0	4.18E-04	5.14E-04	0
	C25	1.08E-03	0	6.61E-04	4.40E-04	0	3.27E-04	3.40E-04	0

	C26+	6.73E-03	0	4.76E-03	1.67E-03	0	9.71E-04	1.45E-03	0
Alkyl-benzenes	*Benzene*	0	0	0	0	0	0	0	0
	C1	4.99E-03	4.20E-03	1.81E-03	5.14E-02	1.56E-02	6.45E-03	2.52E-02	1.66E-02
	C2	5.57E-03	2.08E-02	0	2.21E-02	3.04E-02	8.97E-03	1.39E-02	2.48E-02
	C3	8.82E-03	5.25E-02	0	2.87E-02	6.07E-02	1.29E-02	2.33E-02	5.13E-02
	C4	7.88E-03	5.27E-02	0	2.33E-02	5.47E-02	1.03E-02	1.93E-02	4.95E-02
	C5	5.02E-03	3.73E-02	0	1.08E-02	5.15E-02	5.67E-03	1.06E-02	2.85E-02
	C6	2.99E-03	2.06E-02	0	6.92E-03	1.58E-02	3.54E-03	6.07E-03	1.55E-02
	C7	3.43E-03	2.43E-02	0	6.33E-03	1.48E-02	3.43E-03	4.79E-03	1.67E-02
	C8	3.61E-03	1.83E-02	5.66E-04	4.09E-03	1.20E-02	2.37E-03	4.23E-03	8.61E-03
	C9	3.94E-03	9.03E-03	2.06E-03	3.84E-03	4.81E-03	3.04E-03	3.57E-03	4.69E-03
	C10	3.83E-03	2.98E-03	3.35E-03	3.13E-03	0	2.13E-03	3.17E-03	1.23E-03
	C11	2.79E-03	7.21E-04	2.20E-03	1.83E-03	0	1.43E-03	1.49E-03	4.94E-04
	C12	4.12E-03	8.55E-05	4.58E-03	2.85E-03	0	2.01E-03	2.17E-03	0
	C13+	1.18E-02	0	1.85E-02	2.74E-03	0	2.24E-03	3.90E-03	0
Alkyl-naphthalenes	*C0*	3.72E-04	2.79E-03	0	1.60E-03	3.64E-03	7.64E-04	3.02E-04	3.05E-03
	C1	1.85E-03	1.40E-02	0	9.02E-03	1.62E-02	5.61E-03	9.13E-03	1.39E-02
	C2	5.37E-03	3.21E-02	5.27E-04	2.32E-02	3.35E-02	1.45E-02	2.04E-02	2.88E-02
	C3	1.59E-02	2.71E-02	1.05E-02	5.83E-02	2.53E-02	4.47E-02	4.91E-02	2.25E-02
	C4+	9.77E-02	1.43E-03	1.23E-01	1.06E-01	0	7.64E-02	8.31E-02	0
Total Mass Fraction (g/g %)		**34%**	**80%**	**20%**	**65%**	**73%**	**35%**	**54%**	**70%**